The Tauonic Branching Ratio of $\Upsilon(1S)$

by

Ha Son Lam

B.S., Washburn University at Topeka 1985

M.S., University of Kansas at Lawrence 1988

Submitted to the Department of Physics and Astronomy and the Faculty of the Graduate School of the University of Kansas in partial fulfillment of the requirements for the degree of Doctor of Philosophy.

Dissertation Committee:

____
Chairman

____

____

____

____

____

Date Defended: __________

Abstract

Ha S. Lam, December 1994

University of Kansas

We have studied the leptonic decay of the $\Upsilon(1S)$ resonance into tau pairs using the CLEO II detector. A clean sample of tau pair events is identified via the 1-vs.-1 topology where exactly one of the charged particles is an identified electron. We find $B(\Upsilon(1S) \to \tau^+\tau^-) = \left(2.61 \ \pm \ 0.12 \ {}^{+0.09}_{-0.13}\right)\%$. The result is consistent with expectations from lepton universality.

To my parents

Acknowledgments

First and foremost, I would like to express my deepest thanks to my advisor, Professor Phil Baringer, for his guidance, encouragement, and support. I am also indebted to Professor Ray Ammar for his guidance, encouragement, and support. I would also like to express my thanks to the other members of my dissertation committee: Professors Alice Bean, Peter Hierl, and Douglas McKay.

I have benefited from discussions with other faculty members of the High Energy Physics Group at the University of Kansas, namely Professors Dave Besson, Robin Davis, and Nowhan Kwak. I am also grateful for the assistance of the members of the University of Kansas group stationed at Cornell's Wilson Laboratory: Steven Ball, Don Coppage, Peter Haas, Ned Hancock, Michael Kelly and Nader Copty.

The work described in this dissertation would not have been possible without the effort of the CESR staff and CLEO collaboration; a large number of people helped provide the data that forms the basis of this analysis. In particular I am indebted to Mike Athanas, Jun Masui and Mike Sivertz for much valuable advice and guidance in the trigger studies for my analysis.

Finally, I would like to thank my parents for their love and their encouragement of my career. My brother, Long Lam, has been a constant source of encouragement and support, while my friend, Nhung Nguyen, has been a source of inspiration and support during the data analysis and the writing of this dissertation.

List of Figures

19. $\frac{E_{bump}}{p}$ for π's from K_s^0's

20. $\frac{E_{bump}}{p}$ for π^+'s from data and MC

21. $\frac{E_{bump}}{p}$ for π^+'s from hadron and $\tau^+\tau^-$ MC

22. R_2 of hadrons from $\Upsilon(1S)$

23. n_{ch}, $\Upsilon(1S)$ hadrons

24. n_{neut}, $\Upsilon(1S)$ hadrons

List of Tables

1. Introduction

The theory that most people believe today describing fundamental particles and their properties is known as the Standard Model[1−3](SM). (A complete treatment of the Standard Model can be found in the references.) We now believe that there are four basic forces in nature: gravity, weak, electromagnetic and strong. The Standard Model describes the weak, electromagnetic and strong forces in terms of quantum field theory; gravity can not yet be described in this way. The weak and electromagnetic forces were combined into one (by S. Weinberg[4] and A. Salam[5]) known as the electroweak interaction.

Fundamental particles are classified by their spin: fermions have half-integral spin (in units of $\hbar$), bosons have integral spins. Today we believe that all stable matter is built up from fermions (spin 1/2). These fermions are considered fundamental since they behave like point-like particles. No visible structure is observed from them. According to their interactions, these fermions are grouped into two types: leptons are fermions that interact through the electroweak force; quarks interact through both electroweak and strong forces. In the Standard Model there are three families of leptons and three families of quarks:

$$\begin{pmatrix} e \\ \nu_e \end{pmatrix} \begin{pmatrix} \mu \\ \nu_\mu \end{pmatrix} \begin{pmatrix} \tau \\ \nu_\tau \end{pmatrix}$$

$$\begin{pmatrix} u \\ d \end{pmatrix} \begin{pmatrix} c \\ s \end{pmatrix} \begin{pmatrix} t \\ b \end{pmatrix}$$

These fermions were all directly or indirectly observed including the t quark which has been claimed recently to have mass $M_t = 176 \pm 8 \pm 10$ GeV/c^2 by the

CDF collaboration,[6] and $M_t = 199\ ^{+19}_{-21} \pm 22$ GeV/c^2 by the D0 collaboration.[7]. All of these elementary particles have corresponding anti-particles. Properties of leptons and quarks are shown in Tables 1 and 2, respectively.

Lepton	Charge (Q/e)	Mass (MeV/c^2)
e	-1	0.511
ν_e	0	$<$ 0.0000051
μ	-1	105.7
ν_μ	0	$<$ 0.27
τ	-1	1777
ν_τ	0	$<$ 31

Table 1: Properties of leptons

Quark flavor	Charge (Q/e)	Mass (GeV/c^2)
u	2/3	0.002 to 0.008
d	-1/3	0.005 to 0.015
s	-1/3	0.100 to 0.300
c	2/3	1.0 to 1.6
b	-1/3	4.1 to 4.5
t	2/3	170 to 200

Table 2: Properties of quarks

Force	Field Quanta	Mass (GeV/c^2)	Range (meters)	Coupling Constant	Relative Strength
Gravity	graviton	0	∞	G_N	10^{-33}
Weak	W$^\mp$, Z^0	80.1, 91.2	10^{-18}	G_F	10^{-5}
Electromagnetic	photon (γ)	0	∞	α	10^{-2}
Strong	gluon	0	$< 10^{-15}$	α_s	1

Table 3: Forces and Mediators

Rules for the behavior of the forces can be interpreted as having particles interact through the exchange of four types of gauge bosons: γ, W$^\mp$, Z^0 for the electroweak force and gluons (g) for the strong force. Properties of forces and their mediators are shown in table 3. The exchange of charged gauge bosons W$^\pm$ is called a charged weak current.

The theory of the weak interaction defines three left handed quark doublets and six right handed quark singlets,

$$\begin{pmatrix} u \\ d' \end{pmatrix}_L \begin{pmatrix} c \\ s' \end{pmatrix}_L \begin{pmatrix} t \\ b' \end{pmatrix}_L \text{and } u_R \quad c_R \quad t_R \quad d_R \quad s_R \quad b_R$$

where the subscript denotes the handedness of the doublets. The singlet states do not participate in weak interactions. The weak eigenstates d', s', b' are linear superpositions of strong eigenstates d, s , and b. The u, c, and t quark, by convention, do not mix. The mixing of strong eigenstates can be expressed in terms of the Cabibbo-Kobayashi-Maskawa (CKM) matrix[8] (V) as

$$\begin{pmatrix} d' \\ s' \\ b' \end{pmatrix} = \begin{pmatrix} V_{ud} & V_{us} & V_{ub} \\ V_{cd} & V_{cs} & V_{cb} \\ V_{td} & V_{ts} & V_{tb} \end{pmatrix} \begin{pmatrix} d \\ s \\ b \end{pmatrix} .$$

This CKM matrix is a 3x3 matrix which can be completely specified by four free parameters, one of which is a complex phase. It is believed that this complex phase is the mechanism for CP violation in the K^0 system. Work is now under way to study CP violation in the B^0 system with accelerators known as B factories.

In spite of the successes of the standard model, many questions still remain unanswered, one of which is:

Is the Standard Model correct?

The work in this paper attempts to partially prove or disprove the model, *i.e.*, to see if the universality of the lepton sector holds. Figure 1a. is a Feynman diagram representing the lowest order of quantum electrodynamic (QED) interaction for $e^+e^- \to f\bar{f}$, where f and $\bar{f}$ are fermion and anti-fermion, respectively. The QED cross section for this process is given by:

$$\sigma(e^+e^- \to f\bar{f}) = \frac{4\pi\alpha^2}{3s} Q_f^2, \tag{1.1}$$

where Q_f is the fermion charge, s is the square of the center of mass energy and α is the QED coupling constant. Apart from s, equation (1.1) depends only on Q_f; the cross section for the process $e^+e^- \to f\bar{f}$ is the same for all charged particles in the lepton sector. This is what is refered to as "lepton universality". Figure 1b. is the Feynman diagram representing the creation and the leptonic decay of an Υ meson (a b quark and a $\bar{b}$ antiquark can combine to form a bound state known as an Υ meson). Since the final state in the graph is the same as for the direct production graph (Figure 1a.) the leptonic width of the Υ must also be the same for all charged leptons.

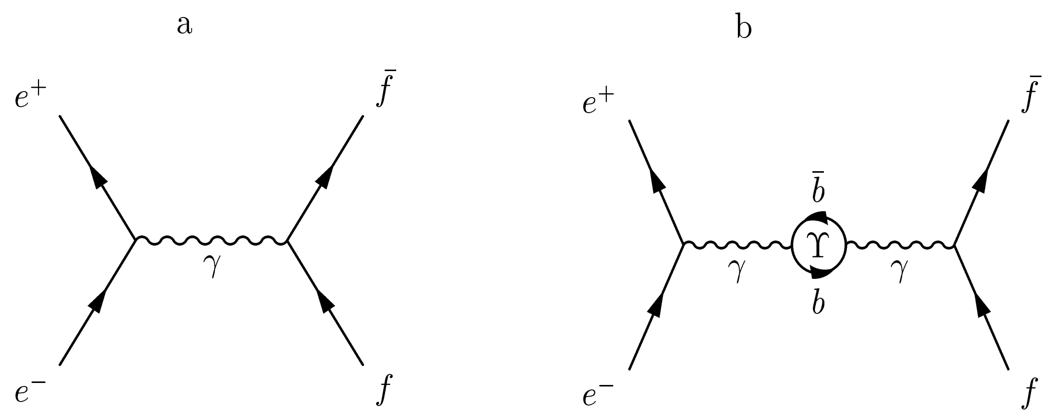

Figure 1. Lowest order QED Feynman diagram for $e^+e^- \to f\bar{f}$ and $e^+e^- \to b\bar{b} \to f\bar{f}$

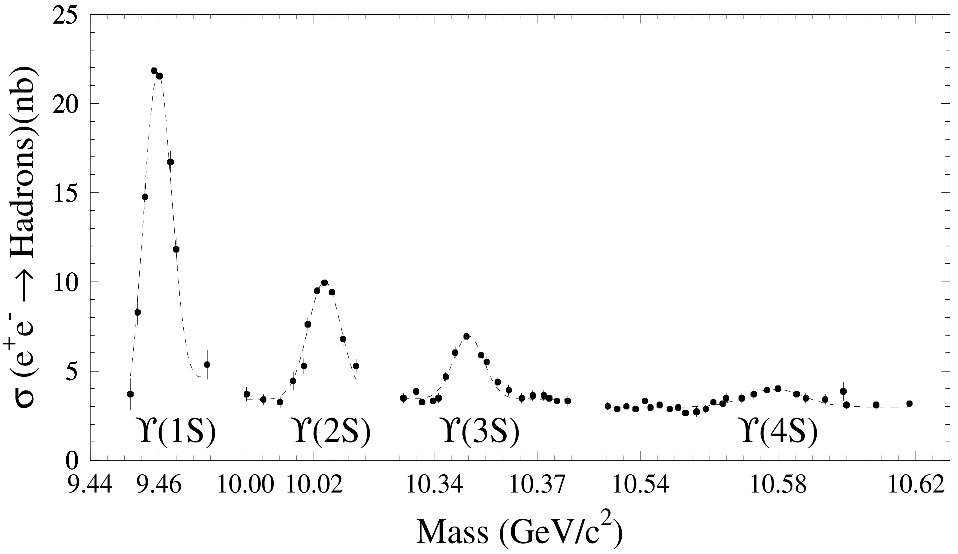

Figure 2. Hadronic cross section for CM energies around 10 GeV from CLEO I.

After the first observation of the Υ family of resonances in proton-nucleus collisions at Fermilab,[10] ARGUS and CLEO started a series of studies of the b meson system through electron-positron collisions at the Υ energy region ($\sim$ 10 GeV). For a $b\bar{b}$ system to be produced directly at an electron-positron collider, it must have $J^{PC} = 1^{--}$ which are the quantum numbers of a virtual photon produced by electron positron annihilation. Figure 2 shows the hadronic cross section for center of mass energies near 10 GeV from the CLEO detector at CESR; the peaks in the figure are associated with the Υ resonances. The Υ(1S), Υ(2S), and Υ(3S) all lie below the energy threshold for decay into pairs of B mesons, so the electromagnetic decays (Figure 1b.) compete with the strong decays due to OZI suppression[1] ("the decays which correspond to disconnected quark diagrams are suppressed"). The measured leptonic decay branching fractions for the bound states are of the order of a few percent. For the Υ(1S), the world average of the branching ratio into tau pairs is $(2.97 \pm 0.35)\%$[11] based on two measurements, one from CLEO[12] and one from ARGUS.[13] There has been one measurement of $B(\Upsilon(2\mathrm{S}) \to \tau^+\tau^-) = (1.7 \pm 1.5 \pm 0.6)\%$ from CLEO.[14] There have been no previous measurements of $B(\Upsilon(3\mathrm{S}) \to \tau^+\tau^-)$. Comparing the tauonic decay rate to those for the e^+e^- and $\mu^+\mu^-$ decay modes is an interesting test of lepton universality. For the Υ(1S), the e^+e^- and $\mu^+\mu^-$ branching ratios have been measured and lie about one standard deviation lower than the tau pair branching ratio. For the Υ(2S), the e^+e^- rate has not been measured, but the muonic and tauonic branching ratios agree within errors. Only the muonic branching ratio of the Υ(3S) has been measured with a world average of $B(\Upsilon(3\mathrm{S}) \to \mu^+\mu^-) = (1.81 \pm 0.17)\%$.[11]

Besides testing lepton universality, these leptonic branching ratios are of additional interest. Taken together with the hadronic widths we can determine the total widths of Υ decays. In principle, one can also extract α_s and the quantum chromodynamic (QCD) parameter Λ by comparing the leptonic branching ratio to the branching ratio to three gluons. The accuracy of this calculation is limited by theoretical uncertainties of higher order QCD corrections and by scale ambiguities, and so we will not present a value of α_s here.

2. The Cornell Electron Storage Ring

The Cornell Electron Storage Ring (CESR) was constructed in 1977-79, and started operating in 1979. CESR provides electron-positron collisions in the energy range of the Υ resonances.

Electrons and positrons are accelerated in a linear accelerator (LINAC) up to 150 MeV and injected into the synchrotron where they remain for about 1 millisecond and are accelerated to about 5 GeV. When desired beam energies are achieved, electrons and positrons are injected into CESR, and continue to circulate around the ring. Positrons are produced by colliding the electron beam about half way through the LINAC with a copper plate; the electrons interact with nucleons through the reaction $e^- + N \to e^- + N + e^+e^-$. Using magnets, the positrons are collected and injected into the synchrotron in the direction opposite that of the electrons. A schematic of the laboratory configuration is shown in Figure 3.

Electron and positron beams in CESR are kept apart by electrostatic separators which have a potential difference of 25,000 volts between the two plates. Near the CLEO interaction region, the separators are turned off, and the beams collide at a small region in CLEO. After about one hour, much of the beam has been lost and CESR is re-filled again. Energy lost to synchrotron radiation in CESR ($\sim$ 1 MeV per particle per turn) is returned to the beams by two radio frequency cavities located on either side of the south interaction region.

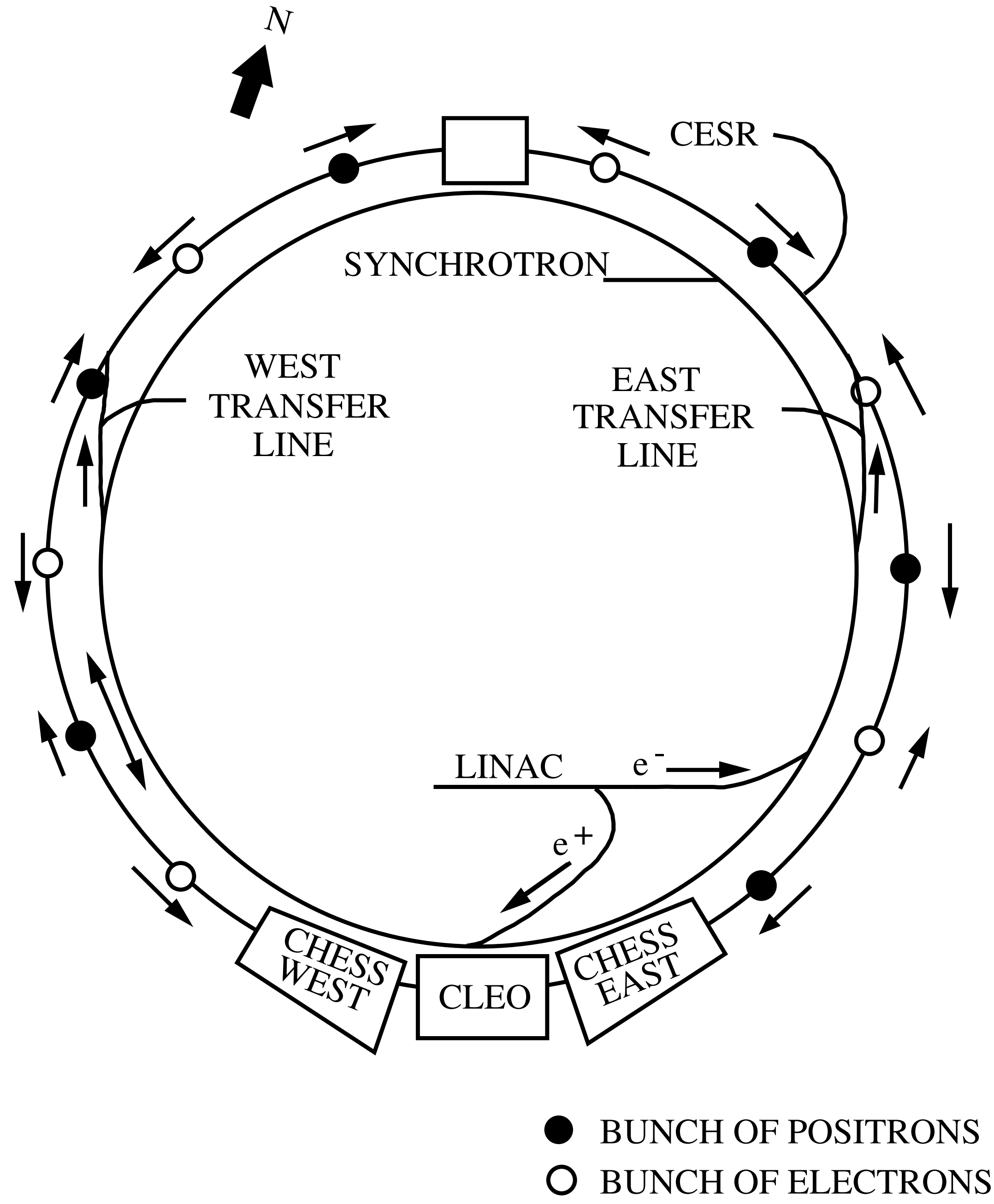

Figure 3. Cornell Electron Storage Ring.

3. The CLEO II detector

In September 1979, two experimental groups, CLEO and CUSB, began recording and analyzing data. The CLEO detector was upgraded to CLEO II in 1988-1989, and data recording began with the new detector in October 1989. A diagram illustrating the CLEO II detector is shown in Figure 4.

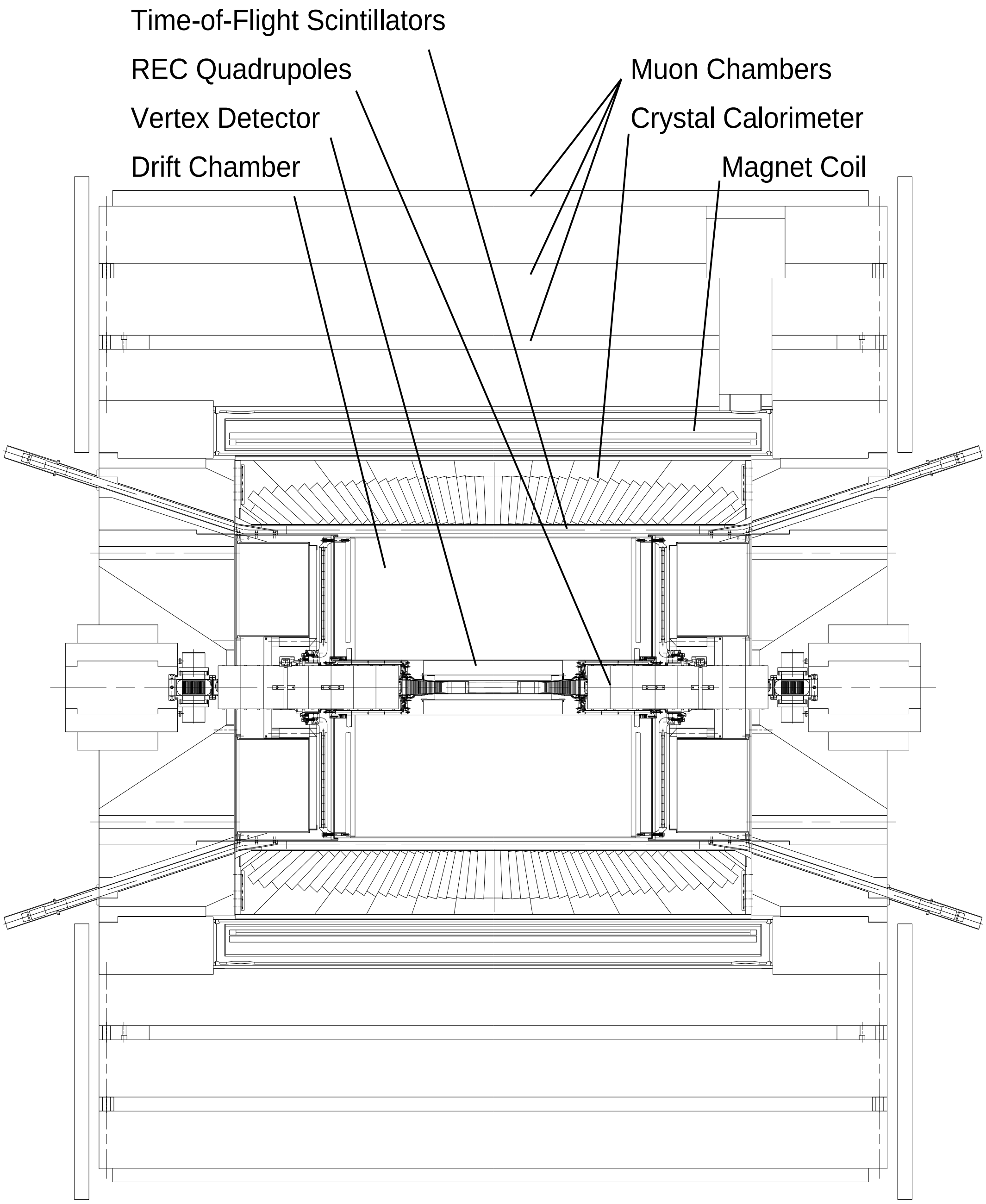

Figure 4. The CLEO II detector (side view).

The CLEO II detector[15] is described in more detail elsewhere. It is a general purpose magnetic spectrometer designed primarily to reconstruct B meson decays. To reconstruct decay events, charged and neutral particles need to be identified and have their momenta measured. The momentum spectrum of interest ranges from under 100 MeV/c for slow π's from $D^* \to D\pi$ to several GeV/c for the π's from $\tau \to \pi\nu$.

Charged particle momenta are measured by their curvature in an axial magnetic field using the central tracking chambers (CD). CD consists of three concentric, cylindrical wire drift chambers: the precision tracking layer (PTL), the intermediate drift chamber (vertex detector, VD) and the outer drift chamber (DR). The momentum resolution is given by

$$\left(\frac{\delta p_t}{p_t}\right)^2 = \left(\frac{53 s p_t}{BL^2\sqrt{n}}\right)^2 + \left(\frac{0.054\sqrt{t}}{BL}\right)^2$$

where s (in meters) is the accuracy of individual position measurements in the drift chambers, p_t is the momentum transverse to the B field in GeV/c, B is the magnetic field strength in tesla, L is the length in meters over which measurements are made, n is the number of position measurements and t is the thickness of obstructing material in the chambers in radiation lengths. Using the formula given above with $B = 1.5$ T, $L = 0.85$ m, $n = 49$, $s = 150\ \mu m$, and $t = 0.025$ r.l. the expected resolution becomes

$$\left(\frac{\delta p_t}{p_t}\right)^2 = (0.0011 p_t)^2 + (0.0067)^2$$

which leads to $\delta p_t = 47$ MeV/c at $p_t = 5.280$ GeV/c. The measured resolution of muon tracks from $e^+e^- \to \mu^+\mu^-$ is 66 MeV/c. This is for p_x and p_y; p_z is less accurately measured.

The energy of neutral particles and electrons is measured in the CsI crystal calorimeter (CC). Charged and neutral particles are separated through a correlation of tracks in the CD with the showers in the crystal calorimeter. The CLEO II crystal calorimeter consists of 7800 thallium-doped cesium iodide (CsI) crystals. The CC energy resolutions for photons are given by

$$\begin{aligned} \text{Barrel}: \frac{\sigma_E}{E}[\%] &= \frac{0.35}{E^{0.75}} + 1.9 - 0.1E \\ \text{Endcap}: \frac{\sigma_E}{E}[\%] &= \frac{0.26}{E} + 2.5, \end{aligned}$$

and the angular resolution is

$$\begin{aligned} \text{Barrel}: \sigma_\phi[mrad] &= \frac{2.8}{\sqrt{E}} + 1.9 \\ \sigma_\theta[mrad] &= 0.8\sigma_\phi \sin\theta, \end{aligned}$$

$$\begin{aligned} \text{Endcap}: \sigma_\phi[mrad] &= \frac{3.7}{\sqrt{E}} + 7.3 \\ \sigma_\theta[mrad] &= \frac{1.4}{\sqrt{E}} + 5.6, \end{aligned}$$

where the photon energy E is in GeV, the barrel region is the detector region with $45° < \theta < 135°$, and the endcap regions are the detector regions with $\theta \leq 45°$ and $135° \leq \theta$. Electrons deposit all of their energy in the calorimeter and so can be identified by comparing E with the momentum p measured in the drift chamber, *i.e.*, $\frac{E}{p} \sim 1$ for electrons and positrons.

Different particles interact differently with matter at low momentum, Figure 5 shows a plot of ionization energy lost (dE/dx) versus particle momentum measured in the CD, the dots are data and the lines are theoretical expectations for the particle types; this provides particle identification at low momentum. Towards the high end of the plot, the dots merge, making distinction among particle types impossible by this method. Flight times from the time of flight (TF) system, and energy deposited in the CC provide other means of particle identification.

The CD, TF, and CC are all contained within a solenoidal superconducting magnet with a magnetic field of 1.5 Tesla. The superconducting coil is cooled by a liquid helium cryogenic system. The magnetic return yoke is formed by three layers of 36 cm thick steel. Each layer is divided into eight symmetrical octants with 9 cm separation between layers for muon detectors. The inner two layers provide almost all of the magnetic flux return. A 2.5 cm thick sheet of steel outside the outermost muon chambers is added for protection and radiation shielding. The magnetic pole pieces are formed of nesting rings on each end of CLEO II to provide magnetic flux return, support structure, access and assembly.

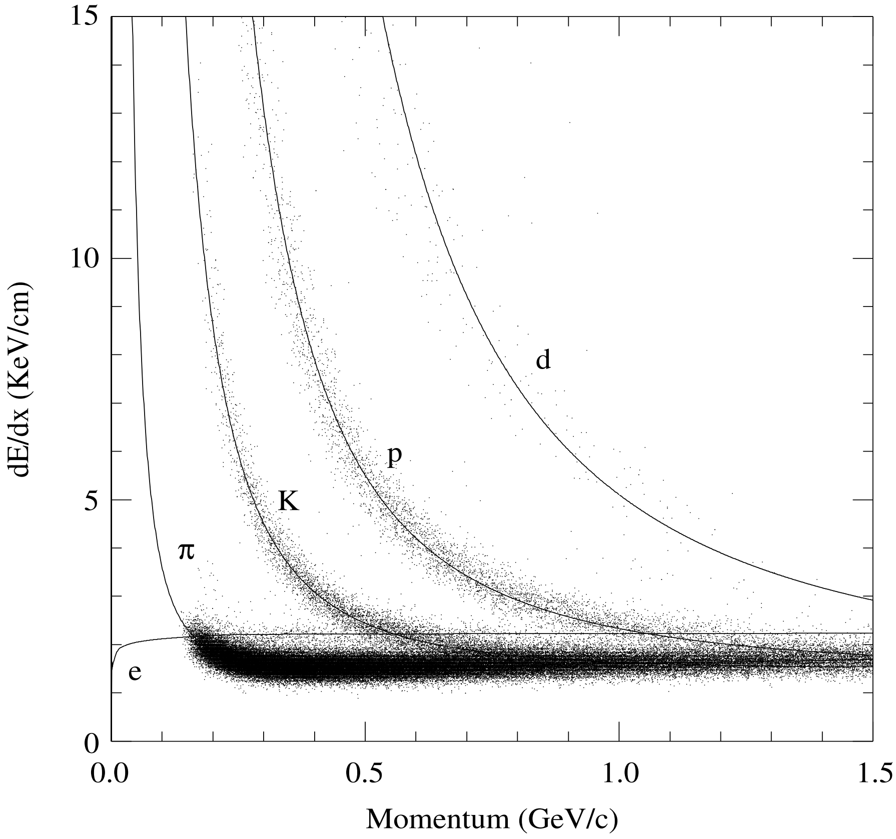

Figure 5. Specific ionization vs track momentum

4. The Analysis

We describe here a new measurement of the tauonic branching ratio of the $\Upsilon(1S)$ which is significantly more precise than the two previous determinations. The analysis method also differs significantly from the previous two analyses. The previous CLEO measurement [12] identified taus in their 1-vs.-3 topology and the ARGUS measurement[13] was based upon $\Upsilon(1S)$ mesons produced via $\Upsilon(2S)$ decays. Here we use data taken on the $\Upsilon(1S)$ resonance and look for tau pair events where one tau has decayed into $e\nu\bar{\nu}$ and the other has decayed into one charged particle which is not an electron (thus a muon, pion, or kaon). This allows us to select a very pure sample of tau pair events and avoid uncertainties associated with the hadronic background. The presence of the electron also improves our understanding of the trigger efficiency of the detector.

The data sample used in this analysis corresponds to an integrated luminosity of 49 pb^{-1} at the energy of the $\Upsilon(1S)$ resonance (the 1S2 dataset). In addition, a 101 pb^{-1} data sample taken in the continuum between the $\Upsilon(3S)$ and $\Upsilon(4S)$ resonances (the 4S4 dataset) is used for background subtraction. The trigger conditions were the same for the two datasets.

5. Event Selection

In measuring the branching ratio we must make a large subtraction to remove the contribution from the nonresonant process $e^+e^- \to \tau^+\tau^-$ from the $e^+e^- \to \Upsilon \to \tau^+\tau^-$ contribution. Also, we must measure the background continuum process at a different energy from the signal process (E_{beam} of 5.263 GeV vs. 4.730 GeV for the Υ(1S)). Therefore we try to choose cuts for which the energy dependence of the efficiency is well simulated by our Monte Carlo. This is the main reason we do not use dE/dx in our particle ID, for example.

In order to reduce non-tau backgrounds each event candidate is required to have two charged tracks, one identified as an electron, e , and the other identified as *not* an electron (we use the notation $\not{e}$ below to denote this track). Determination of the trigger efficiency is critical, so we insist that each event must fire a specific trigger line which we call "ELTRACK_4S4." (We actually use only a portion of the ELTRACK_4S4 line.) This trigger line combines information from the calorimeter and the central drift chamber to identify events with an electron candidates and at least one other charged track. The detailed definition of this trigger and the trigger efficiency determination will be discussed in a later section.

5.1. Electron Identification

match the charged track with energy deposited in the CsI calorimeter. In this paper, the terms bump and (crystal calorimetric) shower are used interchangeably for a region of energy associated with a single particle. "Primary shower" means the shower is not likely to be a shower fragment. The bump and connected region concepts are described in detail elsewhere.[16]

Below, $\vec{p}$ is the measured momentum of the charged track, E_{bump} is the associated energy in the calorimeter.

A track is specified as an electron if:

- There is a matched primary shower.
- There are at most two bumps in the connected region that contains the matched bump. (That is, at most one nearby photon.)
- $0.85 \leq \frac{E_{bump}}{|\vec{p}|} \leq 1.1$.
- There is no associated signal in the muon chambers.

Tracks that fail any of the above criteria are classified as "$\notin$ ".

5.2. Tau Event Selection

The tau event selection cuts are designed to accept two track tau pair events while minimizing the contribution from background processes. Mu pair and Bhabha events can be eliminated by the particle identification criteria (one e, one $\notin$) and by insisting that there be missing energy in the event. Some additional cuts are implemented to reduce the contamination from radiative Bhabhas (such as (d) and (j) below), hadronic events (cut (h) below), and two-photon processes (cut (g) below). The polar angles of the calorimeter bump, and the missing momentum in the event are denoted θ_{bump}, and $\theta_{miss.momentum}$, respectively. E_{vis} is the total visible energy in the event. The event topology cuts applied are:

(a) Exactly two good charged tracks[17] with a net charge of zero.

(b) Both tracks have good matches to calorimeter bumps:

- track - bump matching is unique
- matched bump is a primary bump.

(c) One track must be called "e" and the other "$\not e$" by the electron identification criteria.

(d) At most one track with $|\vec{p}| \geq 0.85 E_{beam}$.

(e) Both tracks satisfy $|\vec{p}| \geq 0.65$ GeV/c.

(f) $\cos(\theta_{bump}) \leq 0.707$ for the matched bumps.

(g) $|\cos(\theta_{miss.momentum})| < 0.98$.

(h) At most 10 isolated bumps.

(i) $20\% < \frac{E_{vis}}{E_{cm}} < 90\%$.

(j) $\frac{\Sigma E_{bump}}{E_{cm}} < -0.36 \frac{|\vec{p}(\not e)|}{E_{beam}} + 0.78$.

(k) $|\vec{p}(e)| < 90\%\ E_{beam}$

$|\vec{p}(\not e)| < 96\%\ E_{beam}$.

Cut (j) is a two-dimensional cut for removing radiative Bhabhas. In Figure 6, $\frac{\Sigma E_{bump}}{E_{cm}}$ is plotted against $\frac{p(\not e)}{E_{beam}}$ for continuum data on which cuts (a) through (i) have been applied. The cluster of events at high $\frac{\Sigma E_{bump}}{E_{cm}}$ and at $\frac{p(\not e)}{E_{beam}}$ of about 0.6 is due to radiative Bhabhas.

These cuts select 4899 events in the $\Upsilon(1S)$ data sample, and 5824 events in the continuum sample. Figure 7 shows the momentum distribution of the electron candidate in our 4S4 continuum events. Normalized $\tau^- \to e^- \overline{\nu}_e \nu_\tau$ Monte Carlo

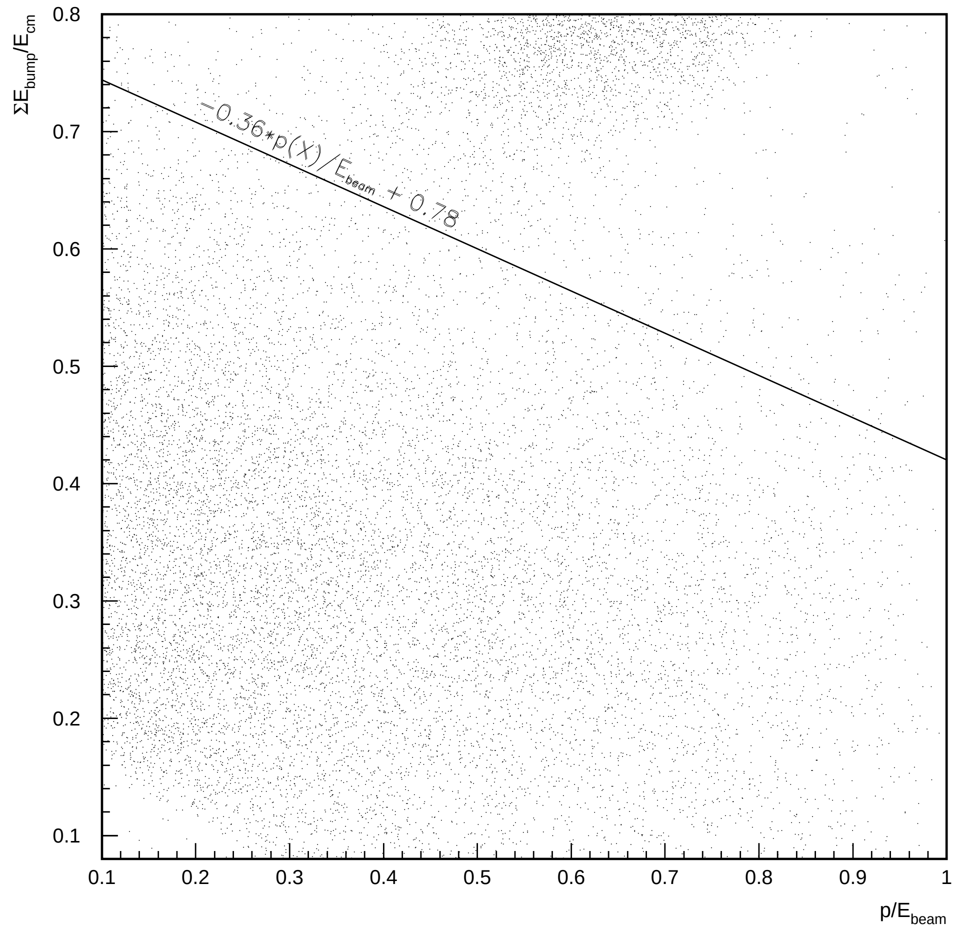

Figure 6. $\frac{\Sigma E_{bump}}{E_{cm}}$ vs. $\frac{p(\not e)}{E_{beam}}$ for continuum data

events agree well with the data. Figure 8 shows the momentum distribution of the $\not e$ tracks for the same data. Figures 9 and 10 show the electron and $\not e$ momentum distributions, respectively, for the 1S2 data. Again, agreement between Monte Carlo and data is good. The tau Monte Carlo curves shown in the figures include the effect of the cuts, but not of any background, misidentification, or trigger efficiency effects. The good agreement with the data, especially at higher momentum, demonstrates that the raw sample has small background and fake contaminations, as we will show in more detail below. The trigger efficiency effects are also addressed below.

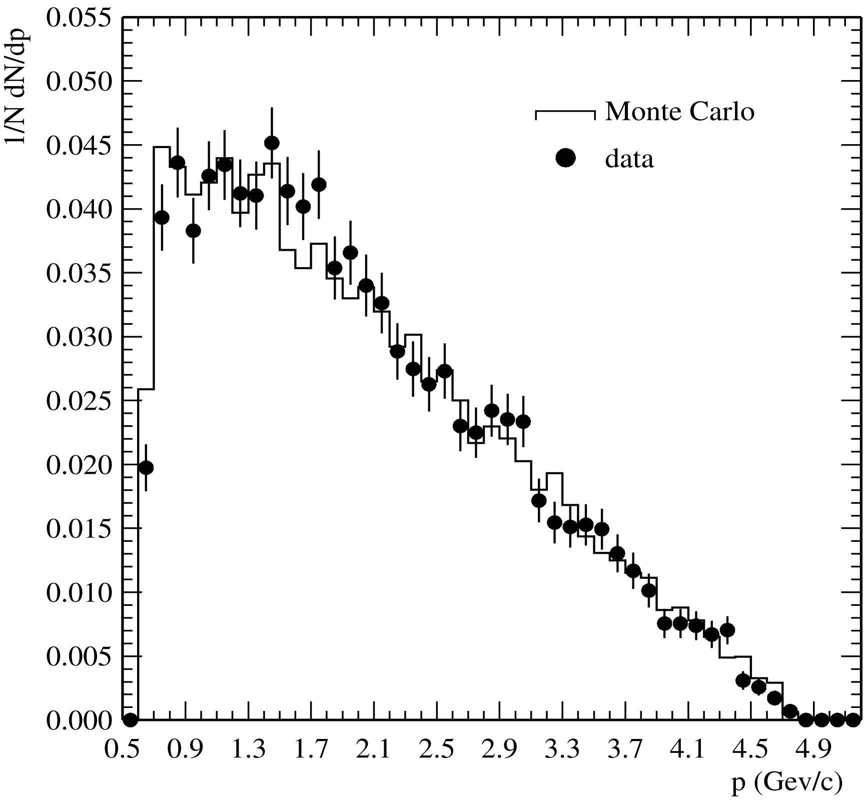

Figure 7. 4S4 Continuum momentum distribution of e

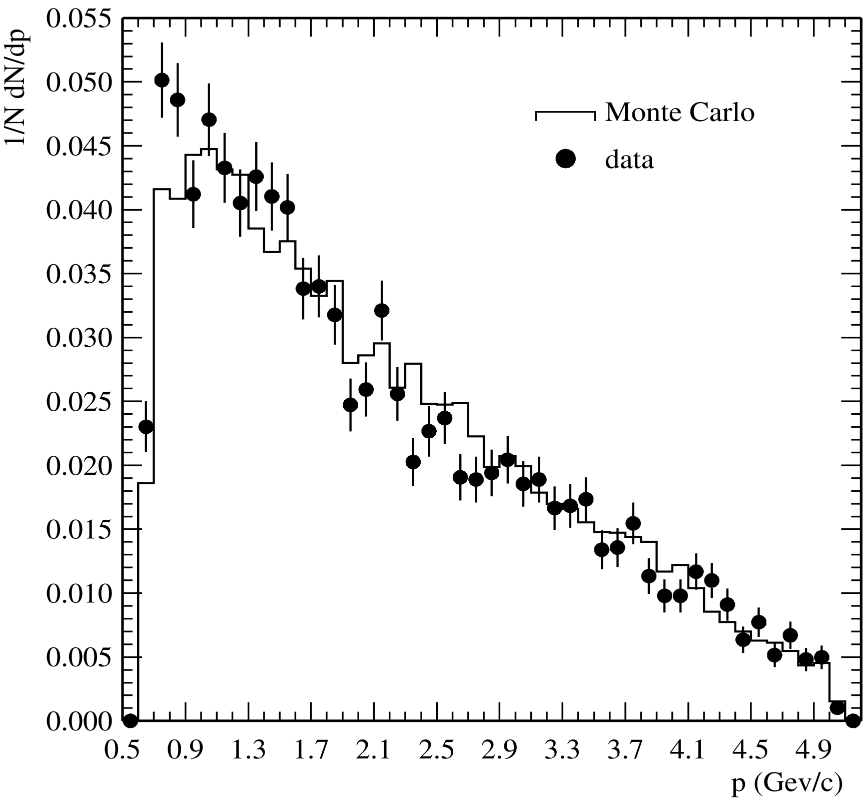

Figure 8. 4S4 Continuum momentum distribution of $\not\ell$

6. Background

A number of background sources were considered. Cosmic rays, μ pairs, beam-wall and beam-gas interactions were investigated using muon chamber, timing, and vertex information. All of these backgrounds were determined to be negligible. Similarly, no radiative Bhabha events passed our cuts when some 20,000 Monte Carlo events were examined. These events were preselected to have the particles in the barrel region of the detector, and correspond to an integrated

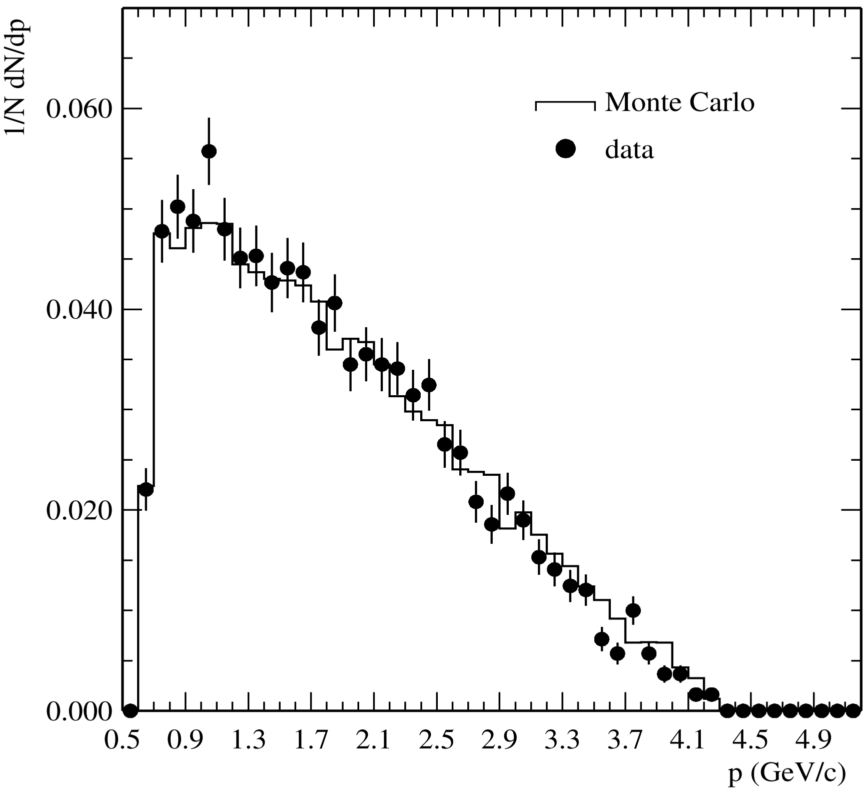

Figure 9. 1S2 momentum distribution of e

luminosity of 33 pb^{-1}.

Potentially, the most significant backgrounds come from hadronic and two-photon ($e^+e^- \to e^+e^-\gamma^*\gamma^*$) processes. About 828,000 fully simulated hadronic continuum Monte-Carlo events were tested, and none passed the cuts. The Monte Carlo sample corresponds to an integrated luminosity of 230 pb^{-1}. In addition, over one million $\Upsilon(1S) \to ggg$ Monte Carlo events were generated. Of these, 28,000 pre-selected events were run through the full detector simulation and only

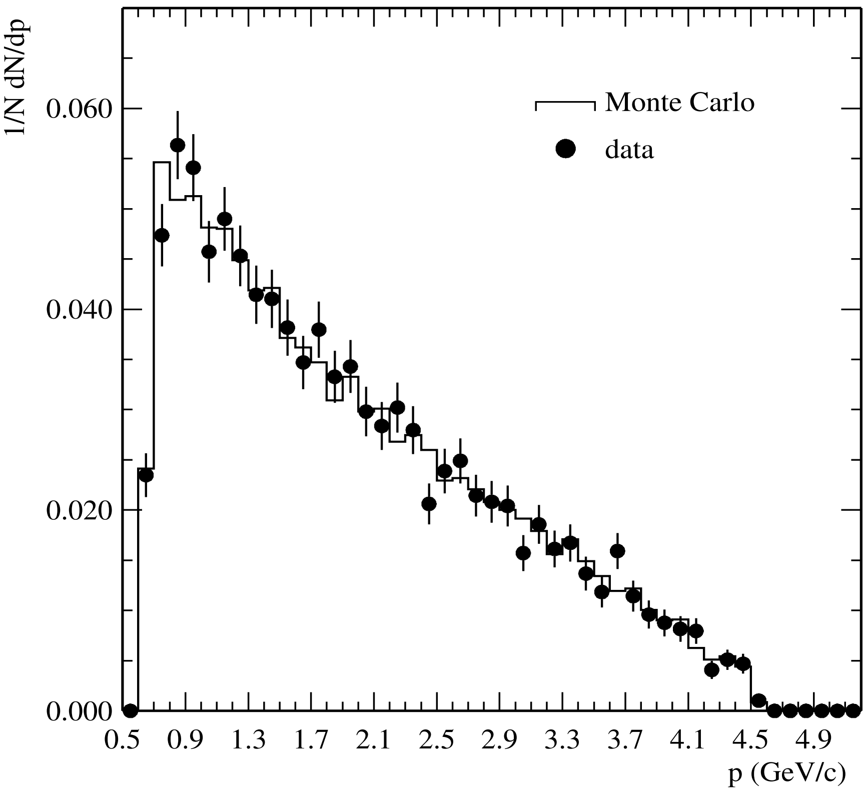

Figure 10. 1S2 momentum distribution of $\not{e}$

one event passed our cuts. Thus we find our hadronic background to be (0.16 $\pm$ 0.01) % which we can safely ignore.

The two-photon cross section does not scale with s (it is basically flat across our range of energies). Monte Carlo data corresponding to 1299 pb^{-1} (19,500 events) with the final state $e^+e^-\tau^+\tau^-$ were examined. There were 364 $\pm$ 18 events that passed our cuts. Based on this value and assuming other two photon processes produce a negligible background, we found 28.3 $\pm$ 1.4 events in our continuum data, and 13.8 ± 0.7 events in the $\Upsilon(1S)$ data. After the continuum subtraction, this background is therefore also negligible, as the 28.3 events scale to 16.1 in the subtraction.

There is also a "background" from real tau events. We expect the signal to include events where one tau decays into $e\nu\bar{\nu}$ and the other tau decays via a mode with one charged particle which is not an electron. We take as the fraction of tau events in our signal process $2B_e(B_1 - B_e)$, where B_1 is the one prong topological branching fraction and B_e is the electronic branching ratio. (We use values for these branching ratios taken from the Particle Data Group.[11]) Tau background is then considered to be any 1-vs.-3 (or 1-vs.-5) tau, or a 1-vs.-1 tau where the e or $\not{e}$ has been misidentified. This background is determined from Monte Carlo (about 100,000 generic tau-pairs from the KORALB[18] generator were put through the full detector simulation), where the electron identification efficiencies have been modified to agree with the data. The determination of the e (and $\not{e}$) fake probabilities is discussed in a later section. The background is most easily expressed as a fraction of the tau-pairs which are "fakes." We found a fake rate of $(4.1 \pm 1.5)\%$ of the $\Upsilon(1S) \to \tau^+\tau^-$ events passing our cuts. Within errors this fake rate is the same on the continuum both under the $\Upsilon(1S)$ and at $E_{beam} = 5.263$ GeV.

7. Trigger Efficiency

Trigger efficiencies were determined from the data because the Monte Carlo trigger simulation did not completely match the data. We describe here the procedures and results of our trigger efficiency determination. Several trigger mnemonics are used in this chapter. They are:

2TFBAR means two opposite TF signals in barrel region.

1TFBAR means one TF signal in barrel.

VD means a signal in vertex detector.

1TRACK means one track with $|p| > 180 MeV$ in CD.

1CBH means one high signal ($> \sim 500$ MeV) in barrel CC.

1PD means a signal in the VD signifying a track.

CBOPP means opposite CC signals in barrel.

BBCBH means high barrel Bhabha signal in CC.

PASS means anything will pass.

PS means prescale with a specified factor.

RADBHA_BCC means radiative Bhabha event tag using barrel CC.

SKRADB means another radiative Bhabha event tag.

7.1. The 1S2 Trigger

The CLEO II trigger has been described in detail elsewhere[19−22]. There are three levels of hardware triggers known as L0, L1, and L2, in order from the fastest to the slowest. Each level has several elements associated with different subsystems of the CLEO II detector. A trigger “line” consists of a set of elements for each of the three trigger levels. In the 1S2 data-taking eleven trigger lines were defined. As stated earlier, we employ a subset of the "ELTRACK_4S4" trigger line (line 4). We impose off-line our own trigger which contains most of the basic components of the ELTRACK_4S4 line. The ELTRACK_4S4 line consists of:

L0: 2TFBAR

L0: 1TFBAR VD

L1: 1TRACK 1TFBAR 1CBH

PS: 1

L2: 1PD.

In this trigger specification, all elements in a row above must fire to satisfy that level. So for level 1, 1TRACK, 1TFBAR, and 1CBH must all be true. When two separate rows appear for a given level, either may be true to satisfy the conditions of the line for that level. So here we must either have 2TFBAR alone or 1TFBAR together with VD at level 0. The notation "PS" stands for the prescaling factor. "PS: 1" means all triggers satisfying line 4 are accepted.

Our off-line trigger requirement is:

2TFBAR*1TRACK*1CBH*1PD.

Thus we are choosing the first of the L0 options in line 4 and not the second. This is due to the uncertainties in determining the VD element efficiency. (1TFBAR is automatically satisfied if 2TFBAR is satisfied.)

All trigger element efficiencies were studied through radiative Bhabha events except for the 2TFBAR efficiency which was studied in the $e\not{E}$ events themselves. Radiative Bhabha events were selected from the 1S2 dataset via the event classifications RADBHA_BCC or SKRADB. The strategy is generally to look at events which fired a different trigger line which does not contain the element under study and measure the fraction of those events that fire the given element. We use trigger line 5 (ENERGY_4S4) to study 1TRACK and 1PD. This trigger line contains:

L0: CBOPP

L1: BBCBH

PS: 1

L2: PASS.

This trigger looks only at energy deposited in the crystal calorimeter and is independent of the other detector subsystems.

7.2. 2TFBAR

The trigger element 2TFBAR uses the barrel time-of-flight scintillators which lie between the central tracking and the crystal calorimeter. 1TFBAR means that one element of the barrel time-of-flight counter has a signal, and 2TFBAR means that two elements have a signal.

To determine the 2TFBAR trigger efficiency, we looked at the number of tau pair events that satisfy both 2TFBAR and VD against the number of events that have 1TFBAR and VD set. (Recall that the L0 of line 4 does not fire on 1TFBAR alone, but also requires VD (a track in the vertex detector). The VD efficiency divides out in our ratio.) We require here a certain minimum pulse height in the ADC. The resulting efficiencies are given by:

$\epsilon_{1TFBAR} = \frac{N_{2TFBAR*VD}}{N_{1TFBAR*VD}}$

$$\epsilon_{2TFBAR} = {\epsilon_{1TFBAR}}^2$$

In our event sample, 4718 events have elements 2TFBAR and VD fired, 4801 events have 1TFBAR and VD fired. This gives:

$$\epsilon_{1TFBAR} = 0.983 \pm 0.003 \text{ and } \epsilon_{2TFBAR} = 0.966 \pm 0.004.$$

These efficiencies are independent of the momentum of the particle, as shown in Figures 11 and 12. Figure 11 displays the number of events versus the momentum of the $\not e$ particle and Figure 12 shows the momentum of the electron candidate. In each figure the top plot shows the events satisfying 2TFBAR*1VD, the middle plot 1TFBAR*1VD, and the bottom plot the ratio of the two. The bottom plots are quite flat within statistics.

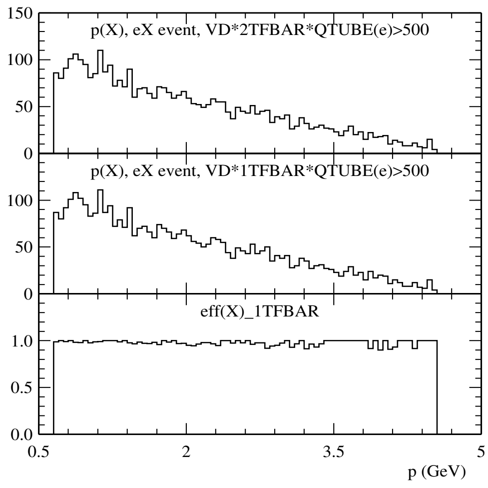

Figure 11. 2TFBAR evts vs. p of $\not e$

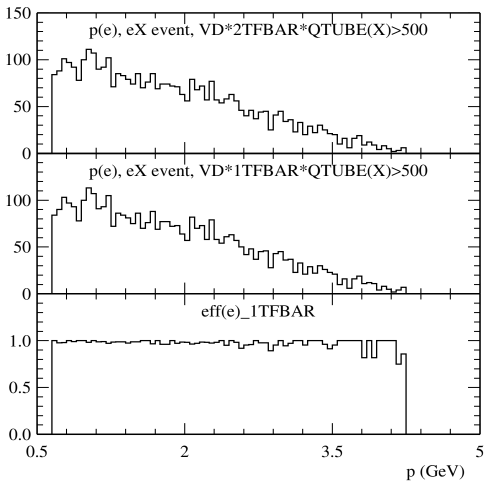

Figure 12. 2TFBAR evts vs. p of e

7.3. 1TRACK

The 1TRACK element is designed to be set "true" if one track with momentum greater than 180 MeV passes through the central tracking system. As a first step in exploring the 1TRACK efficiency, we looked at radiative Bhabha events that fired trigger line 5. Line 5 depends only on the calorimeter and not the central tracking and so is completely independent of the 1TRACK element. Here we also require $cos(\theta_{12}) < 0$, where $cos(\theta_{12})$ is the opening angle between the two tracks. Now we examine how many events have the 1TRACK bit on in our sample. Let x be the ratio:

$$x = \frac{N_{line5*1TRACK}}{N_{line5}}.$$

In our event sample, 14557 events satisfy line 5*1TRACK and 14562 pass line 5, giving $x = 0.9997$. The binomial error on x is negligible. As with 2TFBAR, we find this ratio to be independent of momentum as shown in Figure 13. The events in the figure are binned versus the momentum of the lower momentum track. The top plot shows the events passing line 5*1TRACK, the middle those passing line 5, and the bottom plot shows the ratio, which is quite flat with momentum.

Note that both tracks are electrons in these radiative Bhabha events. A previous trigger study[23] has shown that there is a species dependence for the 1TRACK efficiency. If the efficiencies for the e and $\not{e}$ tracks differ, then the correct event efficiency is:

$$\epsilon_{1TRACK} = \epsilon_e + \epsilon_{\not{e}} - \epsilon_e \cdot \epsilon_{\not{e}} = \epsilon_e + \epsilon_{\not{e}}(1 - \epsilon_e).$$

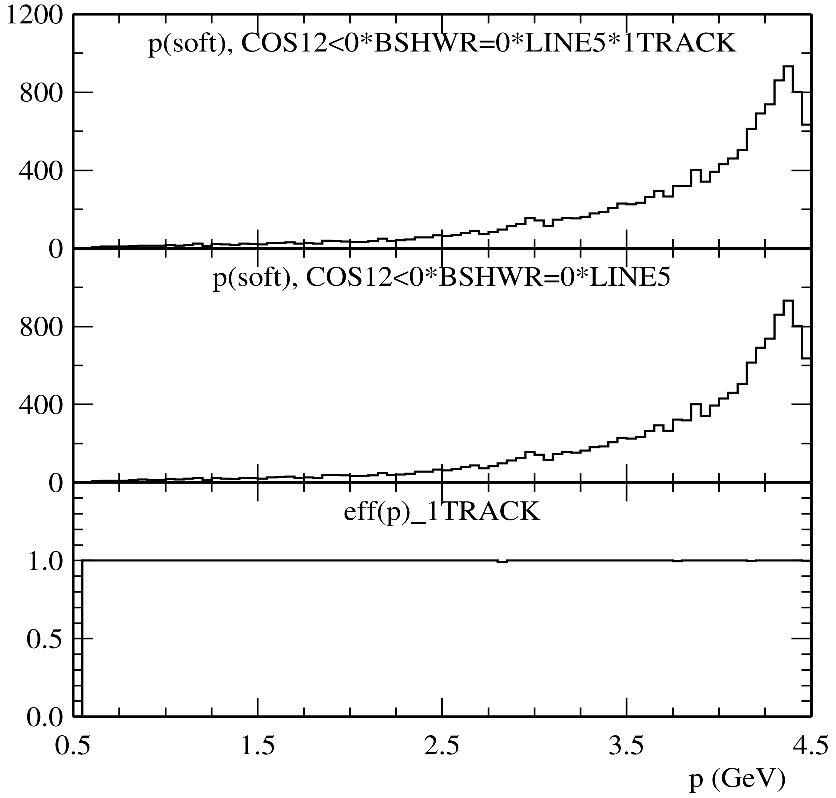

Figure 13. 1TRACK events vs. p of softer e

So, if ϵ_e is large, and we have shown that it is, we are relatively insensitive to the value of $\epsilon_{\not{e}}$. In the previous study, single track efficiencies for 1TRACK were found to be roughly 95% for electrons and 80% for pions, which implies an overall event efficiency of 99%, slightly lower than that found for the radiative Bhabhas. We conservatively assume a 1% error on this efficiency and so we have:

$$\epsilon_{1TRACK} = 0.99 \pm 0.01.$$

7.4. 1PD

The 1PD trigger element uses wire hits in the vertex detector (VD) to look for patterns signifying a track. To determine the efficiency of this trigger element, we again used radiative Bhabha events that fired trigger line 5. We also insisted that events have 2TFBAR set to insure that we are independent of the VD at levels 0 and 1. (1PD is a level 2 element.) We compared the number of events that fired line 5, 1PD, and 2TFBAR, with the total number of events that fired line 5 and 2TFBAR. In our sample, 13629 events passed the line 5*2TFBAR*1PD condition and 13655 events passed line 5*2TFBAR. So, the 1PD efficiency is then:

$$\epsilon_{1PD} = \frac{N_{line5*2TFBAR*1PD}}{N_{line5*2TFBAR}} = 0.9981 \pm 0.0004.$$

As with 2TFBAR and 1TRACK, we find this ratio to be independent of momentum, as shown in Figure 14. The events in the figure are binned versus the momentum of the lower momentum track. The top plot shows the events passing line 5*2TFBAR*1PD, the middle those passing line 5*2TFBAR, and the bottom plot shows the ratio, which is quite flat with momentum.

Thus three of our four trigger elements have efficiencies which are independent of momentum in the momentum region of interest. (Recall that all tracks in our tau sample were required to have a momentum larger than 0.65 GeV. We have only studied the momentum dependence of these three trigger efficiencies for $|\vec{p}| > 0.60$ GeV/c.) We combine our three trigger efficiencies and their errors

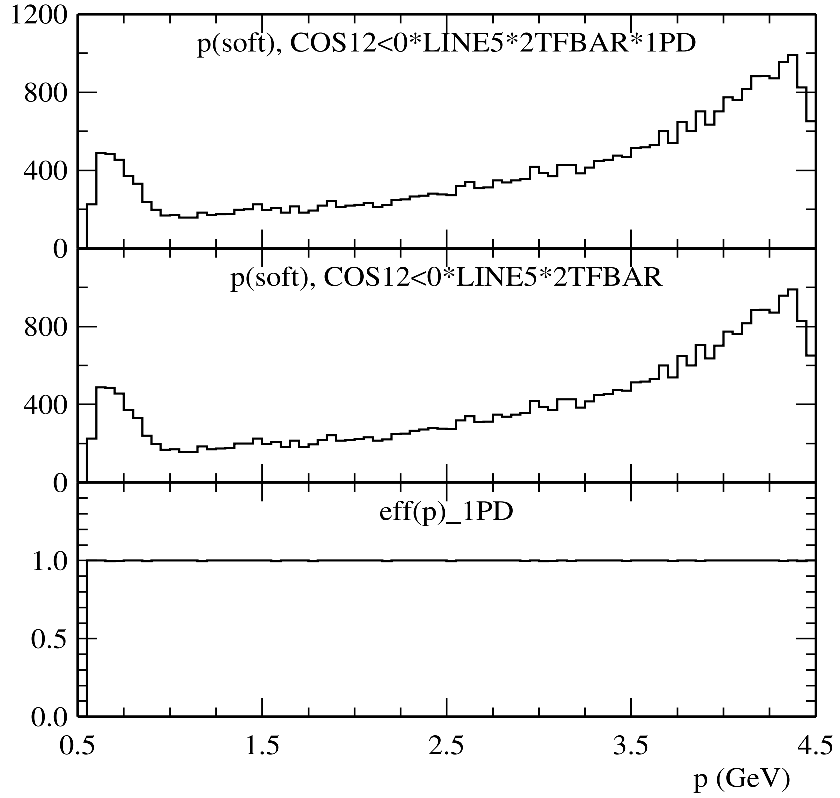

Figure 14. 1PD events vs. p of softer e

into one number:

$$\epsilon_{2TFBAR*1TRACK*1PD} = 0.955 \pm 0.010.$$

7.5. 1CBH

The 1CBH trigger element comes from the crystal calorimeter and requires that a high trigger bit be set somewhere in the barrel region. This corresponds to an energy threshold of roughly 500 MeV. To determine the 1CBH efficiency we again turn to our radiative Bhabha events, but we now also require that the photon not be in the barrel region. That is, the only showers in the barrel region of the calorimeter must be the two associated with the electron tracks. We also require $cos(\theta_{12}) < 0$, as we did in the 1TRACK analysis. We look at another trigger element, 2CBH, which is fired when there are two high energy showers. Assuming the higher momentum track always sets the crystal barrel high bit, we can determine the 1CBH efficiency by counting the number of events that satisfy 2CBH, the number satisfying 1CBH, and taking the ratio:

$\epsilon_{1CBH} = \frac{N_{2CBH}}{N_{1CBH}}$.

We found that this efficiency depends strongly on momentum. Figure 15 shows, plotted versus the momentum of the softer of the two tracks, the number of events satisfying 2CBH (top), the number satisfying 1CBH (middle), and the ratio (bottom). Above a momentum of 0.95 GeV the ratio is flat, but below that the efficiency decreases with decreasing momentum. In Table 4 we give N_{1CBH}, N_{2CBH}, the 1CBH efficiency, and the overall trigger efficiency ($\epsilon_{trig} = \epsilon_{1CBH*2TFBAR*1TRACK*1PD}$), in different momentum bins. The last bin extends from 1.10 GeV out to the beam energy and the 1CBH efficiency is 100% throughout that bin.

To calculate our total trigger efficiency we must combine these values in Table

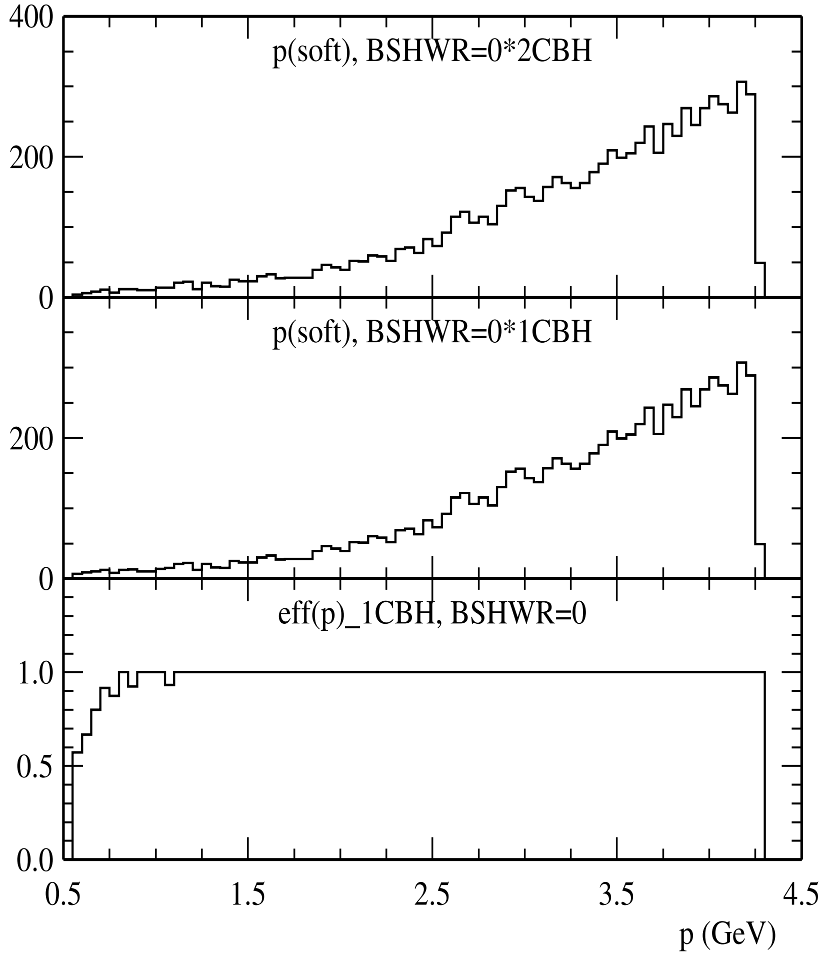

Figure 15. 1CBH events vs. p of softer e

4 with the electron momentum distribution of our tau events. We first fit the efficiencies to two different functions, a polynomial of order three and a threshold function. The fit shown in Figure 16 is to the threshold function:

$$\epsilon_{trig} = N x^n e^{a_1 x + a_2 x^2},$$

p (GeV/c)	N_{1CBH}	N_{2CBH}	ϵ_{1CBH} (%)	ϵ_{trig} (%)
0.65	14	12	85.7 $\pm$ 9.3	81.8 $\pm$ 8.9
0.70	13	12	92.3 $\pm$ 7.4	88.1 $\pm$ 7.1
0.75	11	10	90.9 $\pm$ 8.7	86.7 $\pm$ 8.3
0.80	15	15	100.0 $\pm$ 0.0	95.5 $\pm$ 1.0
0.85	18	17	94.4 $\pm$ 5.4	90.1 $\pm$ 5.2
0.90	13	13	100.0 $\pm$ 0.0	95.5 $\pm$ 1.0
0.95	15	15	100.0 $\pm$ 0.0	95.5 $\pm$ 1.0
1.00	20	20	100.0 $\pm$ 0.0	95.5 $\pm$ 1.0
1.05	16	15	93.8 $\pm$ 6.1	89.5 $\pm$ 5.9
1.10	7678	7678	100.0 $\pm$ 0.0	95.5 $\pm$ 1.0

Table 4: Trigger Efficiency versus Electron Momentum

$$x = (p - \text{offset})$$

where the values obtained from the fit are listed in Table 5.

N	$power(n)$	a_1	a_2	offset
0.99 $\pm$ 0.08	0.020 $\pm$ 0.034	-0.06 $\pm$ 0.14	0.023 $\pm$ 0.054	0.650

Table 5: Parameters from Fit to Trigger Efficiency Momentum Function

Using the fitted function, we take a Monte Carlo generated momentum distribution for the electrons in our tau events and calculate a momentum integrated

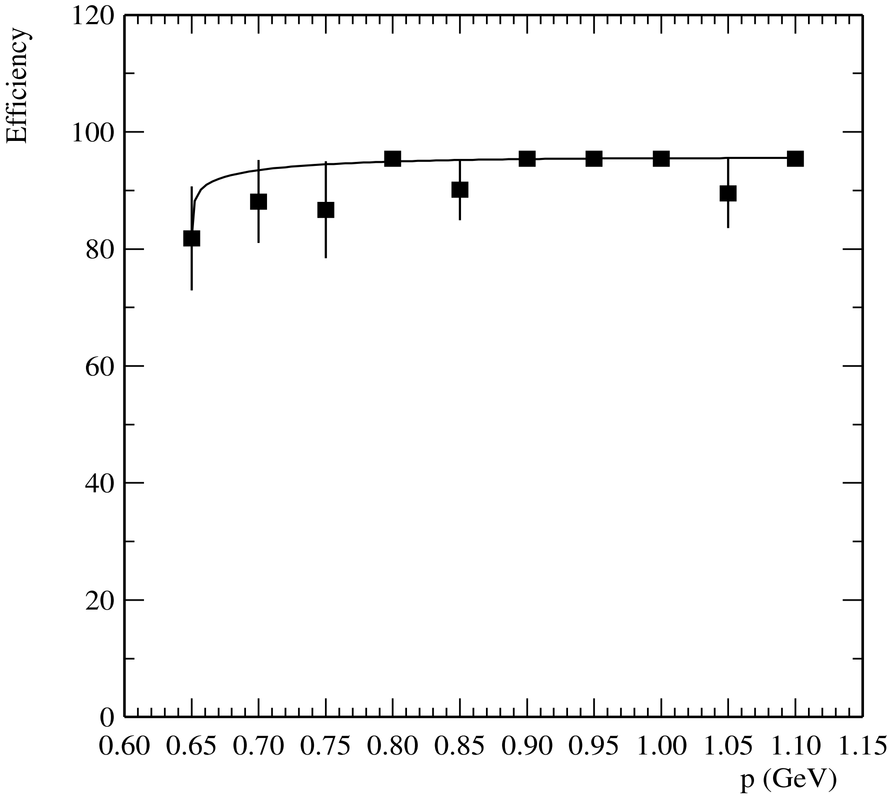

Figure 16. ϵ_{trig} vs. electron momentum

trigger efficiency. We used a constant efficiency of 95.5% above a momentum of 0.95 GeV, and the fitted function at lower momentum. Momentum distributions were generated for continuum produced taus at a beam energy of 5.263 GeV (superscript "*5.2*" below), and 4.730 GeV (superscript "*und*"). Also a momentum distribution for $\Upsilon(1S) \to \tau^+\tau^-$ was generated (superscript "Υ " below). The three momentum distributions are slightly different and give these slightly different efficiencies:

$\epsilon_{trig}^{\Upsilon} = (95.1 \pm 1.2)\%$, $\epsilon_{trig}^{und} = (95.2 \pm 1.4)\%$, $\epsilon_{trig}^{5.2} = (95.4 \pm 1.1)\%$.

The errors on these efficiencies come from the previously quoted errors on the 2TFBAR, 1TRACK, and 1PD efficiencies, plus a 0.6% error on the momentum-integrated 1CBH efficiency. This latter error was determined by observing the spread in values obtained by using different fitting functions and varying the efficiencies in Table 4 within their errors.

In the calculation of the number of tau events, the ϵ_{trig}^{und} and $\epsilon_{trig}^{5.2}$ values appear only in their ratio. This ratio was seen to be quite insensitive to the method of integration over momentum. (The ratio would be one if it were not for the momentum dependence of the 1CBH trigger element.) From the maximum variations in its value, we found the error in this ratio to be 0.2%, and we use: $\frac{\epsilon_{trig}^{und}}{\epsilon_{trig}^{5.2}} = (0.998 \pm 0.002)\%$.

8. Fake Rate

In order to understand what fraction of the tau events we have detected, we need an accurate simulation of our electron identification. The critical cut is: $0.85 < \frac{E_{bump}}{|\vec{p}|} < 1.1$. Muons are very unlikely to deposit this fraction of their energy in the electromagnetic calorimeter, but hadrons occasionally do. As discussed below, we found that our Monte Carlo underestimated by about 50% the fraction of pions which would fake an electron. Thus we use the data itself to determine this fraction. (We assume that any differences between kaons and pions are negligible for this purpose since the $\not{e}$ tracks will be dominantly pions. The tau events cannot contain protons.)

An earlier, independent analysis[24] using a different cluster finding and track matching algorithm (CCFC) obtained fake rates for the cut $0.85 < \frac{E_{bump}}{|\vec{p}|}$ by looking at tracks from tau events. A pure sample of pions was obtained by imposing dE/dx cuts and using muon chamber information. The fake rates found in this study for the $\frac{E_{bump}}{|\vec{p}|}$ cut are given in Table 6. The results are averaged over pion charge and the quoted errors are statistical only. Above a momentum of 2 GeV the π^+ and π^- were seen to give the same fake probability, but at lower momentum they differed.

We pursued our own independent determination of the fake probabilities for our cluster finding method and our $\frac{E_{bump}}{|\vec{p}|}$ cut. We obtain our pions from K_s^0 decays in hadronic events. We compared the values of $\frac{E_{bump}}{|\vec{p}|}$ measured by the two cluster finding techniques. The agreement was excellent, so we expect our fake rates to agree with those in Table 6.

p_{low}	p_{high}	π fake (%)
0.50	1.00	2.86 ± 0.13
1.00	1.50	1.33 ± 0.10
1.50	2.00	1.14 ± 0.11
2.00	2.50	1.57 ± 0.15
2.50	3.00	1.26 ± 0.15
3.00	3.50	1.38 ± 0.19
3.50	4.00	0.58 ± 0.12
4.00	4.50	0.63 ± 0.14
4.50	5.00	0.86 ± 0.23

Table 6: Rate for Pion to Fake Electron from Tau Tracks

In the primary K_s^0 selection, we looked for well measured tracks in the barrel region of the detector with good matches to showers in the calorimeter (same as cut (b) in the tau event selection criteria). The tracks had to come from a secondary vertex, located in the $x - y$ plane, but with good matching in the z coordinate. The K_s^0 momentum vector was required to point back to the primary vertex. The z matching and primary vertex matching are combined via a χ^2-like quantity called "CHITX". We required CHITX ≤ 2.5. In Figure 17 below we show the the invariant mass of the K_s^0 candidates, m_K, plotted versus the invariant mass for the Λ interpretation of the secondary vertex, m_Λ. We see a significant band of Λ's that crosses the K_s^0 mass band. We remove the Λ's by removing combinations having $1.10 < m_\Lambda < 1.13$. Without this cut we found we had significant proton contamination which lead to fake rates which were too high (especially in the π^-'s where the antiprotons can leave significant energy in the calorimeter).

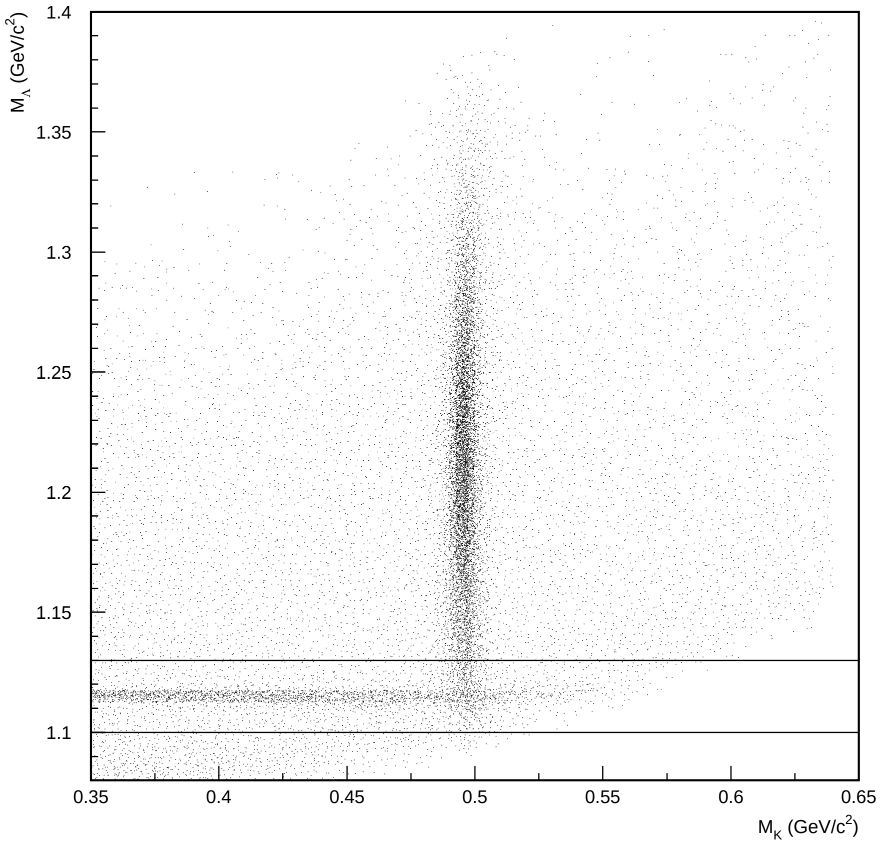

Figure 17. Λ versus K_s^0 invariant mass from data

We next performed three different analyses where we imposed an additional cut on top of the basic set of cuts. In the first analysis we imposed a dE/dx cut, SGPIDI < 0, where SGPIDI is number of sigma away from a pion. This cut selects tracks that deposit less than the expected amount of energy for a pion of that momentum. Hence, this selects away from the region where electrons would appear. (We also required SGPIDI > -10, due to spurious measurements at these extreme values.) In the second and third analyses we impose more restrictive cuts on the quantity CHITX. In Figure 18 we show m_K for the additional cuts SGPIDI < 0 (Figure 18a.), CHITX ≤ 1 (Figure 18b.), and CHITX ≤ 2 (Figure 18c.). We take our pion tracks from those candidates satisfying $0.48 < m_K < 0.51$.

Tables 7, 8, and 9 below give the results found in the three analyses. The "π fake" percentage is determined from the number of tracks passing the cut $0.85 < \frac{E_{bump}}{|\vec{p}|} < 1.1$ (given as "*pass*" in the table), divided by the total number of tracks in that momentum interval (given as "*total*" in the table). We see that the π^+ tracks are more likely to fake electrons than the π^- tracks at lower momentum. Statistics are poor in our sample above a momentum of 1.65 GeV, and we treat the fake rate as flat at momenta higher than this. The errors quoted are binomial errors from the sample statistics.

Figure 19 shows the $\frac{E_{bump}}{|\vec{p}|}$ spectrum for pions from the primary set of K_s^0 cuts with π^-'s shown as the histogram and π^+'s shown as the data points. Figures 20a. through 20f. show the $\frac{E_{bump}}{|\vec{p}|}$ spectra for the π^+'s in the first analysis (with the SGPIDI cut) in different regions of p. The histogram represents the Monte Carlo and the points are the data. We can see here the discrepancy between Monte Carlo and data in the region of the $\frac{E_{bump}}{|\vec{p}|}$ cut. Figures 21a. through 21g. show the $\frac{E_{bump}}{|\vec{p}|}$ spectra for the π^+'s from Monte Carlo. The histogram represents π^+'s from hadronic Monte Carlo and the points represent π^+'s from $\tau^+\tau^-$ Monte Carlo. The plots are nearly identical in each momentum range, indicating that the fake rates determined from the hadronic environment are applicable to the

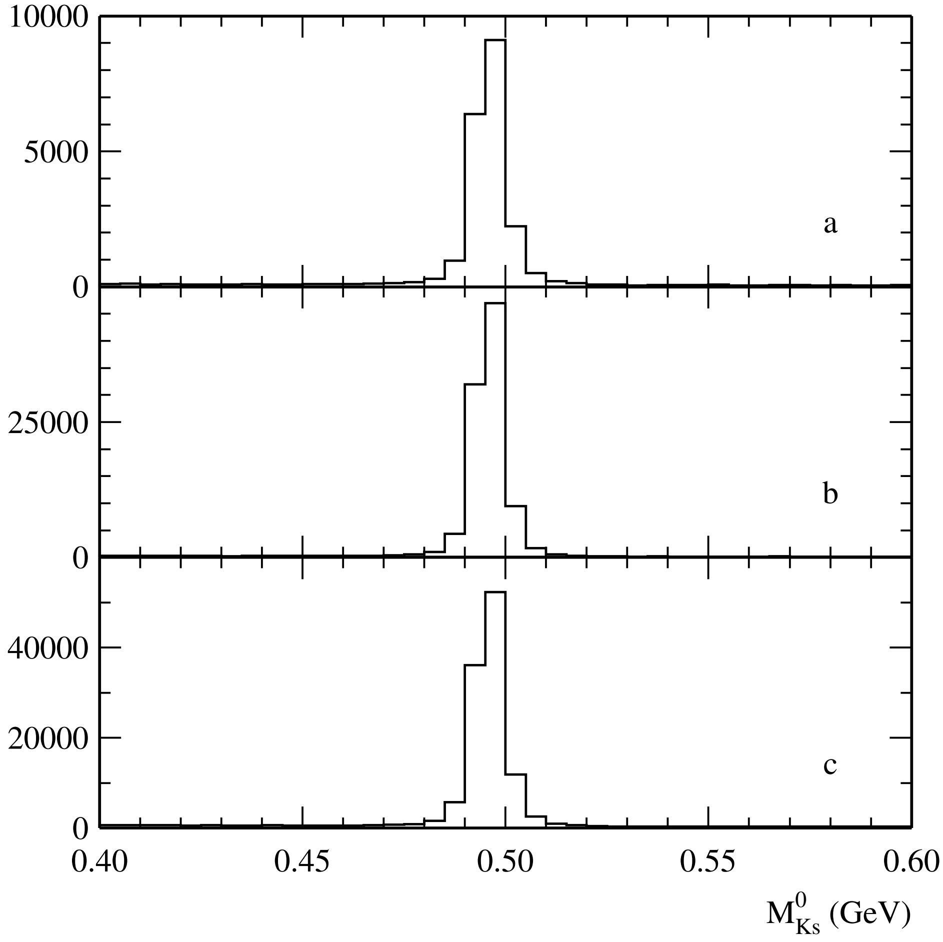

Figure 18. K_s^0 invariant mass peaks for three analyses

$\tau^+\tau^-$'s.

We see that the numbers from the three methods agree well within the statistical errors, so we adopt the values in Table 9, which have the most statistical precision. We can also average these values over charge species and compare to the values in Table 6 from the tau track analysis. The agreement is very good.

p_{low}	p_{high}	$\pi^- \frac{pass}{total}$	π^- fake (%)	$\pi^+ \frac{pass}{total}$	π^+ fake (%)
0.65	0.85	$\frac{91}{5291}$	1.72 ± 0.18	$\frac{333}{7443}$	4.47 ± 0.24
0.85	1.05	$\frac{48}{3621}$	1.33 ± 0.19	$\frac{147}{4549}$	3.23 ± 0.26
1.05	1.25	$\frac{23}{2739}$	0.84 ± 0.17	$\frac{72}{2933}$	2.45 ± 0.29
1.25	1.45	$\frac{21}{1776}$	1.18 ± 0.26	$\frac{27}{1851}$	1.46 ± 0.28
1.45	1.65	$\frac{7}{1021}$	0.69 ± 0.26	$\frac{10}{1083}$	0.92 ± 0.29
1.65	5.00	$\frac{7}{673}$	1.04 ± 0.39	$\frac{2}{633}$	0.32 ± 0.22

Table 7: Rate for Pion to Fake Electron, SGPIDI< 0

p_{low}	p_{high}	$\pi^- \frac{pass}{total}$	π^- fake (%)	$\pi^+ \frac{pass}{total}$	π^+ fake (%)
0.65	0.85	$\frac{229}{13634}$	1.68 ± 0.11	$\frac{631}{13948}$	4.52 ± 0.18
0.85	1.05	$\frac{108}{8133}$	1.33 ± 0.13	$\frac{269}{8296}$	3.24 ± 0.19
1.05	1.25	$\frac{57}{4842}$	1.18 ± 0.16	$\frac{109}{4993}$	2.18 ± 0.21
1.25	1.45	$\frac{34}{3039}$	1.12 ± 0.19	$\frac{46}{2988}$	1.54 ± 0.23
1.45	1.65	$\frac{17}{1749}$	0.97 ± 0.23	$\frac{26}{1846}$	1.41 ± 0.27
1.65	5.00	$\frac{18}{1108}$	1.62 ± 0.38	$\frac{9}{1072}$	0.84 ± 0.28

Table 8: Rate for Pion to Fake Electron, $CHITX < 1$

p_{low}	p_{high}	$\pi^- \frac{pass}{total}$	π^- fake (%)	$\pi^+ \frac{pass}{total}$	π^+ fake (%)
0.65	0.85	$\frac{280}{15647}$	1.79 ± 0.11	$\frac{736}{16003}$	4.60 ± 0.17
0.85	1.05	$\frac{130}{9413}$	1.38 ± 0.12	$\frac{306}{9570}$	3.20 ± 0.18
1.05	1.25	$\frac{75}{5670}$	1.32 ± 0.15	$\frac{131}{5855}$	2.24 ± 0.19
1.25	1.45	$\frac{46}{3577}$	1.29 ± 0.19	$\frac{54}{3532}$	1.53 ± 0.21
1.45	1.65	$\frac{20}{2112}$	0.95 ± 0.21	$\frac{30}{2141}$	1.40 ± 0.25
1.65	5.00	$\frac{22}{1308}$	1.68 ± 0.36	$\frac{14}{1281}$	1.09 ± 0.29

Table 9: Rate for Pion to Fake Electron, $CHITX < 2$

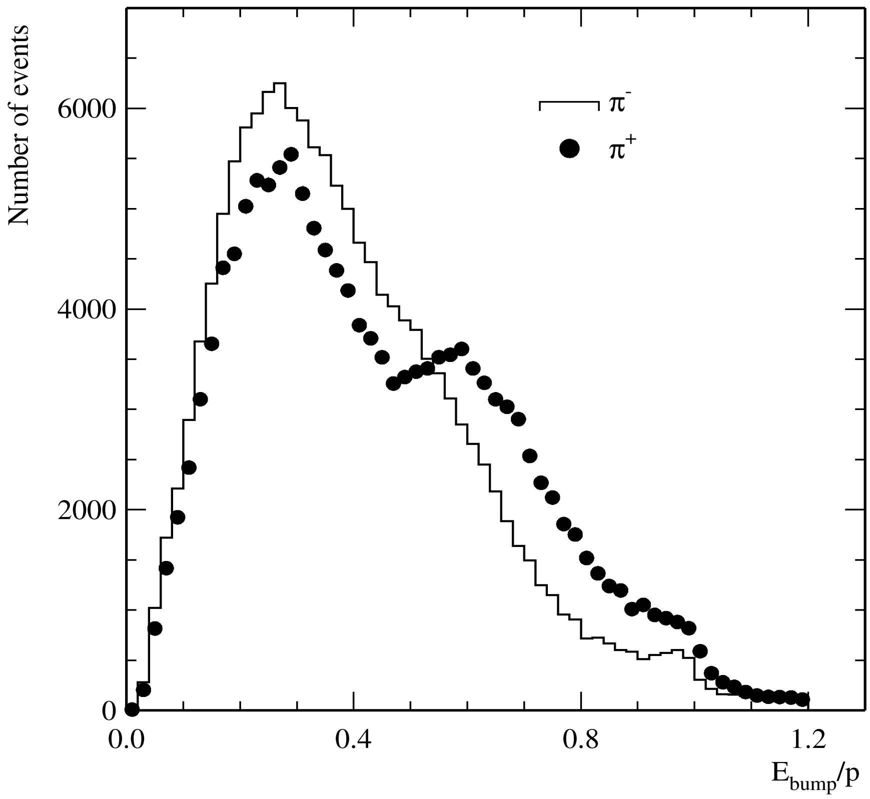

Figure 19. $\frac{E_{bump}}{p}$ for π's from K_s^0's

We now use the values in Table 9 to determine whether a hadron passes the electron identification cut in our Monte Carlo simulation of generic tau events. The simulation then gives us the efficiency of our event selection criteria and the fake rate. We simulate continuum produced taus at beam energies of 5.263 GeV (superscript "*5.2*" below), and 4.730 GeV (superscript "*und*") and taus produced via $\Upsilon(1S) \to \tau^+\tau^-$ (superscript "Υ "). The three momentum distributions are slightly different and give these slightly different efficiencies:

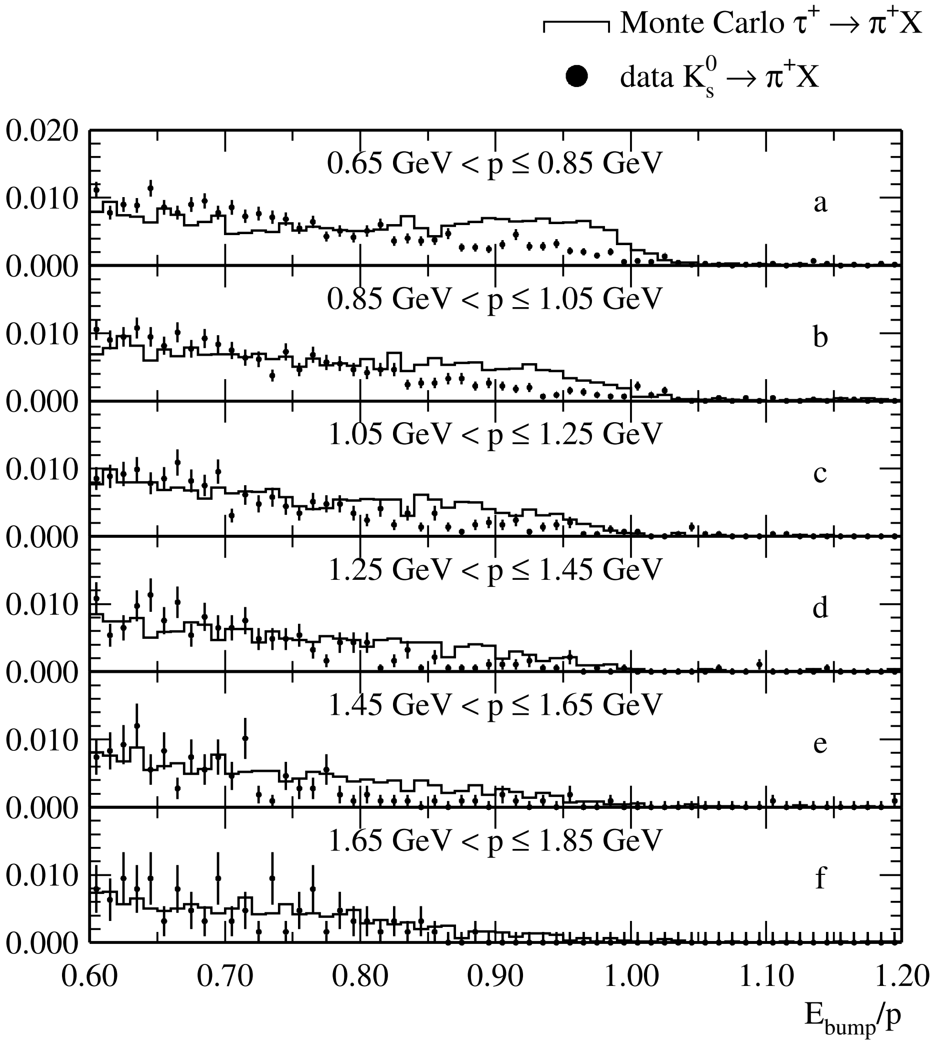

Figure 20. $\frac{E_{bump}}{p}$ for π^+'s from data and MC

$$\epsilon_{e\not e}^{\Upsilon} = (26.69 \pm 0.21)\%, \qquad \epsilon_{e\not e}^{und} = (25.67 \pm 0.17)\%, \qquad \epsilon_{e\not e}^{5.2} = (26.91 \pm 0.17)\%.$$

The errors in these efficiencies come from the Monte Carlo statistics and the uncertainties in the fake rates. The errors on the numbers in Table 9 are statistical only. Additional systematic uncertainties have been added to account for possible uncertainties associated with the cluster finding, track matching, and purity of

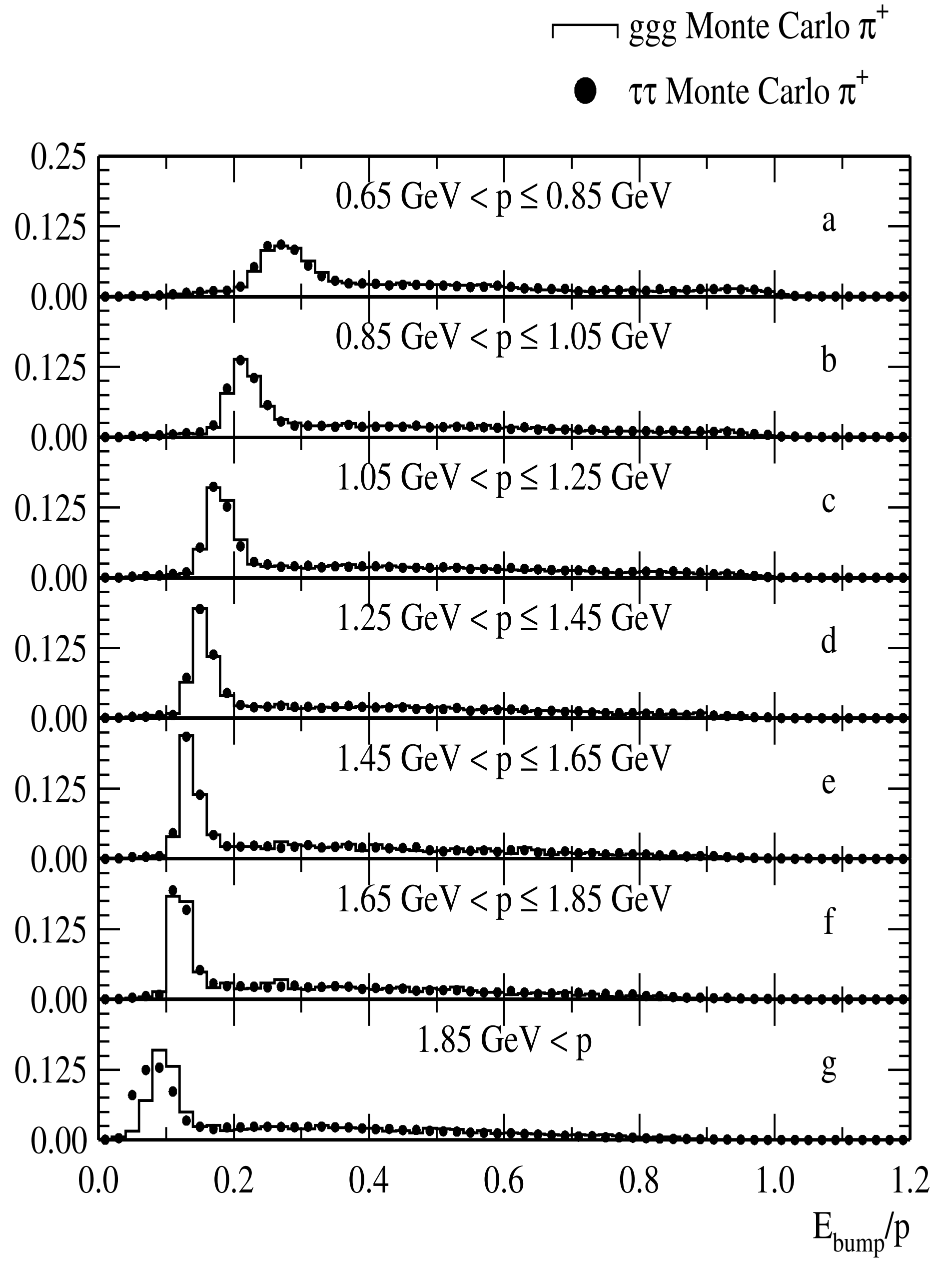

Figure 21. $\frac{E_{bump}}{p}$ for π^+'s from hadron and $\tau^+\tau^-$ MC

the pion samples. Following the earlier study,[24] we assign a 25% systematic error to each value in Table 9 except for the highest momentum bin to which we assign a 50% systematic error. These systematic errors dominate the errors in the fake rates and efficiencies. We obtain for the fake rates:

$$f^{\Upsilon} = (4.1 \pm 1.5)\%, \qquad f^{und} = (4.1 \pm 1.4)\%, \qquad f^{5.2} = (4.1 \pm 1.5)\%.$$

9. Number of Tau Events

We now put together our information on efficiencies, fake rates, and number of events to give us our efficiency corrected, continuum subtracted, number of tau pair events from $\Upsilon(1S)$ decay, N_τ. We use the following formulation:

$$N_\tau = \frac{(N^{4.7}_{raw} - \frac{\epsilon^{und}_{trig}}{\epsilon^{5.2}_{trig}} \cdot \frac{\epsilon^{und}_{e\not{e}}}{\epsilon^{5.2}_{e\not{e}}} \cdot \frac{(1-f^{5.2})}{(1-f^{und})} \cdot \frac{\sigma^{und}_\tau}{\sigma^{5.2}_\tau} \cdot \frac{L^{4.7}}{L^{5.2}} \cdot N^{5.2}_{raw}) \cdot (1 - f^{\Upsilon})}{\epsilon^{\Upsilon}_{trig} \cdot \epsilon^{\Upsilon}_{e\not{e}} \cdot B(\tau^+\tau^- \rightarrow \ e\not{e})},$$

where N_{raw} is the yield of uncorrected tau pair events, f is the fraction of "fake" tau pairs, ϵ is either a trigger efficiency (subscript "*trig*") or a tau event selection efficiency (subscript " $e\not{e}$ "). The superscript "*4.7*" means a quantity is for the $\Upsilon(1S)$ energy; a superscript "*5.2*" is for a quantity at the energy of the data used for continuum subtraction. Superscripts "*und*" and "Υ" are for quantities at the $\Upsilon(1S)$ energy, but the former is for the nonresonant contribution and the latter for events from the resonance. The various values used and the resulting number of tau events are given in the table below.

The quoted systematic error comes from the uncertainties (other than the statistical uncertainties in the raw event yields) listed in Table 10. The column $\frac{dN_\tau}{dx}\sigma_x$ shows the contribution to the statistical or systematic error from the item in the table (statistical above the thick line, systematic below). The uncertainties in the trigger efficiencies and fake rates have been discussed previously. The ratio of the luminosities, L, is known to 0.5%.[25] Luminosities are determined using e^+e^-, $\mu^+\mu^-$, and $\gamma\gamma$ final states by a method which is described in detail elsewhere.[26]

Quantity	Value	$\frac{dN_\tau}{dx}\sigma_x$
$N_{raw}^{4.7}$	4899 ± 70	1089
$N_{raw}^{5.2}$	5824 ± 76	670
f^Υ	$(4.1 \pm 1.5)\%$	401
$\frac{(1-f^{5.2})}{(1-f^{und})}$	0.9998 ± 0.0021	107
$\frac{\epsilon_{trig}^{und}}{\epsilon_{trig}^{5.2}}$	0.998 ± 0.002	102
$\frac{\epsilon_{e\not{e}}^{und}}{\epsilon_{e\not{e}}^{5.2}}$	0.954 ± 0.008	429
$\frac{\sigma_\tau^{und}}{\sigma_\tau^{5.2}}$	1.218 ± 0.006	255
$\frac{L^{4.7}}{L^{5.2}}$	0.4865 ± 0.0024	255
ϵ_{trig}^Υ	$(95.1 \pm 1.2)\%$	317
$\epsilon_{e\not{e}}^\Upsilon$	$(26.69 \pm 0.21)\%$	199
$B(\tau^+\tau^- \rightarrow \; e\not{e})$	$(24.31 \pm 0.27)\%$	275
N_τ	25,100 $\pm$ 1,300 $\pm$ 800	

Table 10: Tau Event Calculation

9.1. Continuum Tau Cross Sections

The tau pair cross sections, σ, which appear in a ratio in our calculation, come from an α^3 QED calculation[27]:

$$\sigma_{\tau\tau} = \frac{86.855\text{nb}}{s} \cdot (1 + \delta(s))$$

and the functional form of $1 + \delta(s)$ is well approximated by

$$1 + \delta(s) = 1.1735 + 0.0303 \cdot (E_{beam} - 5.29) - 0.0060 \cdot (E_{beam} - 5.29)^2$$

The theoretical error on this cross section is 1%. The radiative correction term δ is only weakly energy dependent so we take the ratio of cross sections to have an error of 0.5%. A Monte Carlo calculation of the cross section (which basically does an integral that yields the above expressions) was also done and the ratio of the cross-sections was found to be independent of the cutoff energy of the photon.

10. Hadronic Normalization

In order to measure $B(\Upsilon \to \tau^+\tau^-)$, we must normalize the number of tau events to the total number of events from the Υ(1S) resonance. Here we assume lepton universality, and normalize to the number of hadronic events. We used the same full data sets to determine the number of hadrons and the number of taus from the 1S2, thus minimizing luminosity uncertainties. The continuum data used for subtraction also use the same runs as the tau analysis, but were taken from the data sets that contain only hadron tracks instead. The formula used to obtain the number of hadrons is:

$$N_h = \left(N^{4.7}_{raw,h} - \frac{\epsilon^{und}_h}{\epsilon^{5.2}_h} \frac{\sigma^{und}_h}{\sigma^{5.2}_h} \frac{L^{4.7}}{L^{5.2}} N^{5.2}_{raw,h} \right) \cdot \left(\frac{1 - f^{\Upsilon}_h}{\epsilon^{\Upsilon}_h} \right)$$

where $N_{raw,h}$ is the yield of uncorrected hadronic events, ϵ_h is the hadronic efficiency (trigger and event selection combined), σ_h is the hadronic cross section, and f^{Υ}_h is the fake rate from $\Upsilon(1S) \to \tau^+\tau^-$.

Hadronic event selection was done using a set of cuts designed to optimize efficiency for the ggg decays of the Υ(1S).[28] Events are accepted as hadrons if they meet these criteria: more than two charged tracks, $r-\phi$ position of primary vertex within 2 cm of the beam position, z position of the primary vertex within 5 cm of the beam position, $\Sigma E_{bump} > 0.12 E_{cm}$, $E_{vis} \geq 0.3 E_{cm}$. Events with fewer than five charged tracks, $E_{vis} \geq 0.9 E_{cm}$, and R_2[29] > 0.95 are excluded as likely radiative Bhabhas (R_2 is an event shape variable which distinguishes jetty events from spherical events). The hadron skim cuts were also applied. From Monte Carlo, we find the efficiency for hadrons from the Υ(1S) resonance is 98.8% with these cuts. The efficiency for continuum hadronic events is 94.0% at the Υ(1S) energy and 94.4% at a beam energy of 5.263. The continuum subtracted hadronic yield is found to be 886,600 $\pm$ 1100 events where the error is statistical only. A Monte Carlo calculated tau background of 7300 events was subtracted to arrive at this number. All the values used in this calculation are listed in Table 11.

Quantity	Value	$\frac{dN_h}{dx}\sigma_x$
$N^{4.7}_{raw,h}$	1133422 ± 1065	1068
$N^{5.2}_{raw,h}$	416534 ± 645	389
f^{Υ}_{h}	$(0.822 \pm 0.044)\%$	397
$\frac{\epsilon^{und}_h}{\epsilon^{5.2}_h}$	0.996 ± 0.010	2509
$\frac{\sigma^{und}_h}{\sigma^{5.2}_h}$	1.2381 ± 0.0062	1255
$\frac{L^{4.7}}{L^{5.2}}$	0.4865 ± 0.0024	1255
ϵ^{Υ}_{h}	$(98.8 \pm {}^{+1.2}_{-4})\%$	${}^{+10,765}_{-35,884}$
N_h	$886{,}600 \pm 1100\ {}^{+11,200}_{-36,000}$	

Table 11: Hadronic Event Calculation

The dominant systematic error comes from the determination of the 98.8% efficiency number. We examined the agreement between the Monte Carlo simulation and the continuum subtracted hadronic data. In Figures 22, 23, and 24 below we show the R_2 [29], charged multiplicity, and neutral multiplicity distributions. The data show an excess at low multiplicity, leading to a possible overestimation of the efficiency. Roughly a third of this excess can be accounted for by the tau

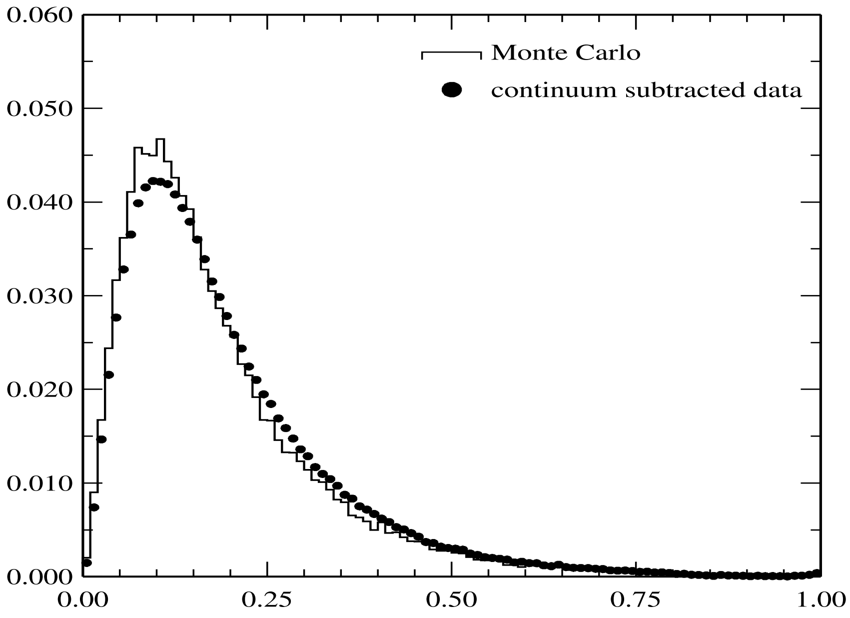

Figure 22. R_2 of hadrons from $\Upsilon(1S)$

contamination in the data. Because the discrepancy tends to produce a lower efficiency and because one cannot have an efficiency in excess of 100%, we assign an asymmetric systematic error of $^{+11{,}202}_{-36{,}017}$ events to the number of hadrons. Revising the cuts to also require either at least five charged tracks or eight or more neutrals produced a change in N_h of only 1.2%, well within our estimated error. The ratio of the continuum efficiencies changed by less than 1%, even though one might expect it to change a bit, justifying the estimated error.

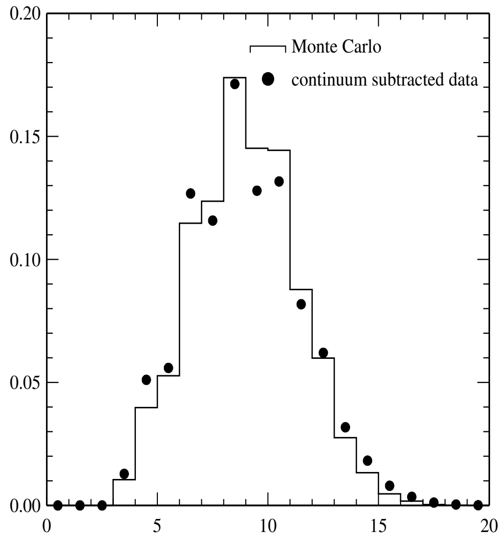

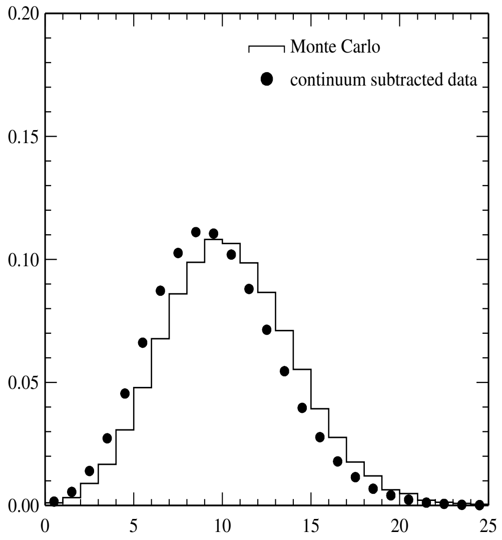

Figure 23. n_{ch}, $\Upsilon(1S)$ hadrons

Figure 24. n_{neut}, $\Upsilon(1S)$ hadrons

11. Results

In obtaining our branching ratio, we first define $\bar{B}$ as the ratio of $\sigma(\Upsilon \to \tau^+\tau^-)$ to $\sigma(\Upsilon \to h)$, where h stands for hadrons. Then, assuming lepton universality:

$$B(\Upsilon \to \tau^+\tau^-) = \frac{\Gamma_{\tau^+\tau^-}}{\Gamma_h + 3\Gamma_{\tau^+\tau^-}} = \frac{\sigma(\Upsilon \to \tau^+\tau^-)}{\sigma(\Upsilon \to h) + 3\sigma(\Upsilon \to \tau^+\tau^-)}$$
$$B(\Upsilon \to \tau^+\tau^-) = \frac{\bar{B}}{1 + 3\bar{B}}$$

We now find $\bar{B}$ from the ratio of the numbers of taus and hadrons reported in previous sections: $\bar{B} = 0.0283 \pm 0.0014^{+0.0010}_{-0.0015}$. This yields the branching ratio:

$$B(\Upsilon(1S) \to \tau^+\tau^-) = \left(2.61 \;\pm\; 0.12 \;\begin{matrix} +0.09 \\ -0.13 \end{matrix}\right)\%.$$

We can test lepton universality by comparing this number to previous measurements of the mu-pair and electron-pair branching ratios. These values are[11]: $B(\Upsilon(1S) \to \mu^+\mu^-) = (2.48 \pm 0.07)\%$, and $B(\Upsilon(1S) \to e^+e^-) = (2.52 \pm 0.17)\%$. We see that our tau branching ratio is in closer agreement with lepton universality than the previous world average.

One can also derive the branching ratio without assuming $\Gamma_{\tau^+\tau^-} = \Gamma_{\mu^+\mu^-} = \Gamma_{e^+e^-}$. Since it is justified by previous measurements, we assume the electron and muon widths are equal, and use the above value for $B_\mu = B(\Upsilon(1S) \to \mu^+\mu^-)$. Then:

$$\begin{aligned}
B(\Upsilon \to \tau^+\tau^-) &= \frac{\Gamma_{\tau^+\tau^-}}{\Gamma_h + \Gamma_{\tau^+\tau^-} + 2\Gamma_{\mu^+\mu^-}} \\
\Gamma_{\mu^+\mu^-} &= B_\mu(\Gamma_h + \Gamma_{\tau^+\tau^-} + 2\Gamma_{\mu^+\mu^-}) \\
B(\Upsilon \to \tau^+\tau^-) &= \frac{\Gamma_{\tau^+\tau^-}}{\Gamma_h + \Gamma_{\tau^+\tau^-} + \frac{2B_\mu}{1-2B_\mu}(\Gamma_h + \Gamma_{\tau^+\tau^-})} \\
B(\Upsilon \to \tau^+\tau^-) &= \frac{\bar{B}(1 - 2B_\mu)}{(1 + \bar{B})}
\end{aligned}$$

This formulation gives a value $B(\Upsilon \to \tau^+\tau^-) = \left(2.62 \ \pm \ 0.13 \ {}^{+0.09}_{-0.13}\right)\%$, so we see that the different universality assumptions have little effect on the end result.

In conclusion, we have measured the tauonic branching ratio of the $\Upsilon(1S)$ resonance. The value we obtain is more precise than previous measurements and is consistent with expectations from lepton universality.

APPENDIX

$\Upsilon(3S)$ Analysis

Our original intent was also to measure the previously unmeasured branching ratio of the $\Upsilon(3S)$ into tau pairs. The muon pair branching ratio has been measured to be $(1.81 \pm 0.17)\%$.[11] Assuming a similar value for the tauonic mode, the continuum background is more than ten times the signal from $\Upsilon(3S) \rightarrow \tau^+\tau^-$. Thus large statistics and a good understanding of the continuum subtraction are needed to make a precise measurement. Unfortunately, we achieved neither of these conditions. We had to restrict ourselves to using just 44 pb^{-1} of the $\Upsilon(3S)$ dataset which were the on-peak runs with stable trigger conditions. Background subtractions were determined from a sample of 197 pb^{-1} taken on the continuum between the $\Upsilon(3S)$ and $\Upsilon(4S)$ (part of the 4S2 dataset). This dataset had different trigger conditions from the $\Upsilon(3S)$.

For continuum subtraction we have to scale our cross sections and efficiencies to the 5.179 GeV beam energy of the $\Upsilon(3S)$ from the continuum beam energy of 5.263 GeV. Our systematic error is dominated by the error in this continuum scaling factor. We assigned a relative error of 3% to this factor, which due to the small signal to continuum ratio results in a large systematic error in the branching ratio. If, for example, one wanted to reduce the systematic error in the branching ratio to 5%, one would need to understand this scaling factor to about 0.2%.

With a slightly different set of cuts (different because this analysis was older) we obtained 1771 events from the $\Upsilon(3S)$ and 8556 from the continuum sample. As in the $\Upsilon(1S)$ analysis all backgrounds were negligible except the two photon background. Here (again, for historical reasons) we subtracted the two photon contribution before continuum subtraction. We subtracted 45.0 ± 2.6 events from the continuum data and 8.5 ± 0.5 events from the $\Upsilon(3S)$ data. Tau feedback was defined a bit differently in this analysis and $(3.3 \pm 0.1)\%$ of the taus were defined as "background" here.

Another background exists which is unique to the $\Upsilon(3S)$ analysis, namely cascade decays to lower mass resonances. The $\Upsilon(3S)$ and $\Upsilon(2S)$ can decay hadronically to lower mass Υ states and radiatively to χ_b states which in turn decay into Υ states. Subsequently, these Υ states can decay leptonically. We calculated this background from a Monte Carlo sample of 39884 generic $\Upsilon(3S)$ decays. The product branching ratio for all decay chains that go from the $\Upsilon(3S)$ to $\tau^+\tau^- X$ which we used was:

$$B(\Upsilon(3S) \to \Upsilon X \to \tau^+\tau^- X) B(\tau^+\tau^- \to e\not{e}) = (1.29 \pm .37) \times 10^{-3}$$

In this Monte Carlo sample four cascade decays pass our cuts. We thus attributed 14.5 ± 3.6 events in our $\Upsilon(3S)$ sample to cascade background.

The branching ratio we calculated was $B(\Upsilon(3S) \to \tau^+\tau^-) = (1.24 \pm 0.67 \pm 0.81)\%$, where we normalized to a $\Upsilon(3S)$ hadronic cross section of 3.248 ± 0.011 nb.[30] The careful trigger and fake rate studies done for the $\Upsilon(1S)$ analysis were not done here. Monte Carlo values were used without correction. We note that the careful studies done on the $\Upsilon(1S)$ changed the central value little (from 2.48% to 2.59%), but reduced the uncertainties considerably. The systematic uncertainty quoted for this $\Upsilon(3S)$ number may be underestimated. The differing trigger conditions between $\Upsilon(3S)$ and continuum and the uncertainty in the $\Upsilon(3S)$ cross section make it hard to reduce the systematics with these data. Given the lack of statistical significance additional effort with these data does not seem worthwhile. We feel this analysis technique is sound and would be worth applying to a larger $\Upsilon(3S)$ data set and accompanying continuum data taken with identical trigger conditions.

REFERENCES

1. D. Griffiths, *Introduction to Elementary Particles*, Wiley (1987).

2. D.H. Perkins, *Introduction to High Energy Physics* Addison Wesley (1982).

3. F. Close, *An Introduction to Quarks and Partons*, Academic Press (1979).

4. S. Weinberg, *Phys. Rev. Lett.* **19**, 1264 (1967).

5. A. Salem, *Elementary Particle Theory: Relativistic Groups and Analyticity (8Th Nobel Symposium)*, edited by N. Svartholm, Almqvist and Wiksell, Stockholm, 1968, p. 367.

6. F. Abe, *et al.* (CDF Collab.), *FERMILAB-PUB-95/022-E.*

7. S. Abachi, *et al.* (D0 Collab.), *FERMILAB-PUB-95/028-E.*

8. M. Kobayashi and T. Maskawa, *Prog. Theor. Phys. (Kyoto)* **49**, 652 (1973).

9. L. Wolfenstein, *Phys. Rev. Lett.* **51**, 1945 (1984).

10. S. W. Herb, *et al.*, *Phys. Rev. Lett.* **39**, 252 (1977).

11. Particle Data Group, L. Montanet *et al.*, *Phys. Rev.* **D50**, 1173 (1994).

12. R. Giles *et al.*, *Phys. Rev. Lett.* **50**, 877 (1983).

13. H. Albrecht *et al.*, *Phys. Lett.* **154B**, 452 (1985).

14. P. Haas *et al.*, *Phys. Rev.* **D30**, 1996 (1985).

15. Y. Kubota *et al.*, *Nucl. Instr. and Meth.* **A320**, 66 (1992).

16. From NOTES (CLEOSOFT), "XBAL documentation", 44: " 'Connected region' is a group of adjacent crystals with $E > 10 MeV$. Crystals are adjacent if they are nearest neighbours, or if they are next-to-nearest neighbors and at least one of them is a local energy maximum in the group of the nearest neighbors. Connected regions are used to describe complexity of a cluster in the calorimeter, which can be produced by one or more photons (or other particles). 'Bump' is a local energy maximum in the group of 9, i.e. corresponds to a crystal with energy larger than any of its nearest neighbors. Any particle (γ,e,μ or even hadron) entering the calorimeter will most likely produce a bump at a place where the calorimeter was intersected first. Bumps are used to assign calorimetric energies (and directions) to individual photons or other particles."

17. A good track is one with |impact parameter with respect to beam spot| < 0.01 m and is a good primary track.

18. `KORALB 2.1/ TAUOLA 1.5`: S. Jadach and Z. Was, *Comput. Phys. Commun.* **36**, 191 (1985) and *ibid*, **64**, 267 (1991); S. Jadach J.H. Kühn, and Z. Was, *Comput. Phys. Commun.* **64**, 275 (1991), *ibid*, **70**, 69 (1992), *ibid*, **76**, 361 (1993).

19. C. Bebek *et al.*, *Nucl. Instr. Meth.* **A302**, 261 (1991).

20. R. Galik, *CBX 89-50*, "Loading Triggers in CLEO II".

21. R. Galik, K. Kinoshita, G. Crawford, *CBX 90-30*, "Adding BLT to Level 1 Triggering".

22. D. Acosta, *CBX 92-32*, “Measurements of the TF and CD Trigger Efficiencies for Two-Track Events”.

23. Darin E. Acosta, “Investigations into Scintillating Fiber Calorimetry and a Measurement of the Two-Photon Production of Charged Meson Pairs”, *Ph.D. Thesis*, U. C. San Diego, 1993.

24. Brian K. Heltsley, *CBX 93-108*, “SEID: A Simple Electron ID Package for Tau Physics”.

25. B. Heltsley, private communication.

26. G. Crawford *et al.*, *Nucl. Instr. and Meth.* **A345**, 429 (1994).

27. Alan Weinstein, private communication.

28. Cuts were obtained via private communication with Dave Besson.

29. G. Fox and S. Wolfram, *Phys. Rev. Lett.* **41**, 1581 (1978).

30. Fran Morrow, private communication.